Long-term imaging of individual ribosomes reveals ribosome cooperativity in mRNA translation

Madern, Maximilian F.; Yang, Sora; Witteveen, Olivier; Segeren, Hendrika A.; Bauer, Marianne; Tanenbaum, Marvin E.

Important note
To cite this publication, please use the final published version (if applicable).
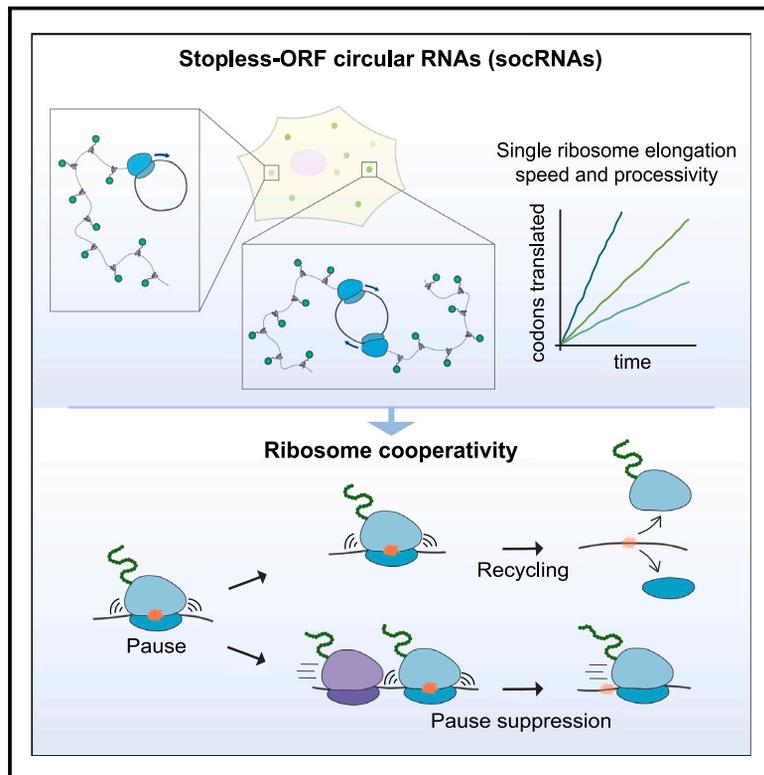Please check the document version above.

Long-term imaging of individual ribosomes reveals ribosome cooperativity in mRNA translation

Graphical abstract

Highlights

- The socRNA technology allows precise measurements of translation elongation dynamics

- Transient ribosome collisions are not sensed by translation surveillance pathways

- Ribosome collisions reduce translational pausing on problematic RNA sequences

- Ribosome cooperativity suppresses stochastic pausing on non-problematic sequences

Authors

Maximilian F. Madern, Sora Yang, Olivier Witteveen, Hendrika A. Segeren, Marianne Bauer, Marvin E. Tanenbaum

Correspondence

m.tanenbaum@hubrecht.eu

In brief

Ribosomes cooperate through transient collisions to ensure efficient translation.

CellPress

Cell

Article

Long-term imaging of individual ribosomes reveals ribosome cooperativity in mRNA translation

Maximilian F. Madern,[1,2,3] Sora Yang,[1,3] Olivier Witteveen,[2] Hendrika A. Segeren,[1] Marianne Bauer,[2] and Marvin E. Tanenbaum[1,2,4,*]

[1]Oncode Institute, Hubrecht Institute—KNAW and University Medical Center Utrecht, Uppsalalaan 8, 3584 CT Utrecht, the Netherlands
[2]Department of Bionanoscience, Kavli Institute of Nanoscience Delft, Technische Universiteit Delft, Van der Maasweg 9, 2629 HZ Delft, the Netherlands
[3]These authors contributed equally
[4]Lead contact
*Correspondence: m.tanenbaum@hubrecht.eu
https://doi.org/10.1016/j.cell.2025.01.016

SUMMARY

The genetic information stored in mRNAs is decoded by ribosomes during mRNA translation. mRNAs are typically translated by multiple ribosomes simultaneously, but it is unclear whether and how the activity of different ribosomes on an mRNA is coordinated. Here, we develop an imaging approach based on stop-less-ORF circular RNAs (socRNAs) to monitor translation of individual ribosomes in either monosomes or polysomes with very high resolution. Using experiments and simulations, we find that translating ribosomes frequently undergo transient collisions. However, unlike persistent collisions, such transient collisions escape detection by cellular quality control pathways. Rather, transient ribosome collisions promote productive translation by reducing ribosome pausing on problematic sequences, a process we term ribosome cooperativity. Ribosome cooperativity also reduces recycling of ribosomes by quality control pathways, thus enhancing processive translation. Together, our single-ribosome imaging approach reveals that ribosomes cooperate during translation to ensure fast and efficient translation.

INTRODUCTION

During mRNA translation, ribosomes translocate along the mRNA one codon at a time, reading the mRNA sequence and synthesizing the corresponding polypeptide chain. Translation of a single codon consists of multiple steps, including decoding (delivery of a cognate amino-acyl tRNA to the ribosomal A-site), transfer of the growing peptide chain from the P-site peptidyl-tRNA to the A-site aminoacyl-tRNA, a reaction that is catalyzed by the peptidyl transferase center of the ribosome, and finally translocation, during which the mRNA is moved relative to the ribosome by one codon.[1] While the canonical translation elongation cycle has been relatively well resolved, ribosomes often encounter difficult-to-translate sequences that alter translation elongation dynamics. Such sequences include both programmed translation pause sites, like sequences that facilitate co-translational protein folding or targeting to organelles,[2,3] as well as RNA structures, nucleotide modifications[4] or even RNA damage.[5,6] How ribosomes resolve such obstacles is poorly understood.

Much of our knowledge on ribosome translocation comes from biochemical and structural studies, in which ribosomes are generally assessed individually.[1,7] However, *in vivo* mRNA molecules are usually translated by multiple ribosomes simultaneously in the form of polysomes, adding an additional layer of complexity that has remained largely unexplored. Different ribosomes within a polysome could undergo different types of functional interactions. One example of a functional interaction between ribosomes has recently emerged; if a ribosome is stalled on a problematic sequence, the trailing ribosome can collide with the stalled ribosome. This collided "disome" flags the leading ribosome as defective, leading to its removal by cellular quality control pathways.[8–11] Moreover, if the number of cellular collided ribosomes is high, a cell-wide stress response is triggered.[12] While ribosome collisions have mainly been studied in the context of a stalled ribosome, it is unknown whether (transient) collisions also occur between two translocating ribosomes within dense polysomes, and if so, what the consequences of such transient collisions are on translation elongation.

While structural, biochemical and sequencing-based approaches have uncovered many key aspects governing ribosome translocation, these approaches generally provide insufficient resolution to map the kinetic landscape of ribosome-ribosome interactions in cells. Previously, our lab and others have developed live-cell single-molecule imaging assays based on fluorescence labeling of nascent polypeptides to visualize translation dynamics with high spatial and temporal resolution in living cells.[13–17] This technology has already led to important insights into the

(legend on next page)

CellPress
OPEN ACCESS
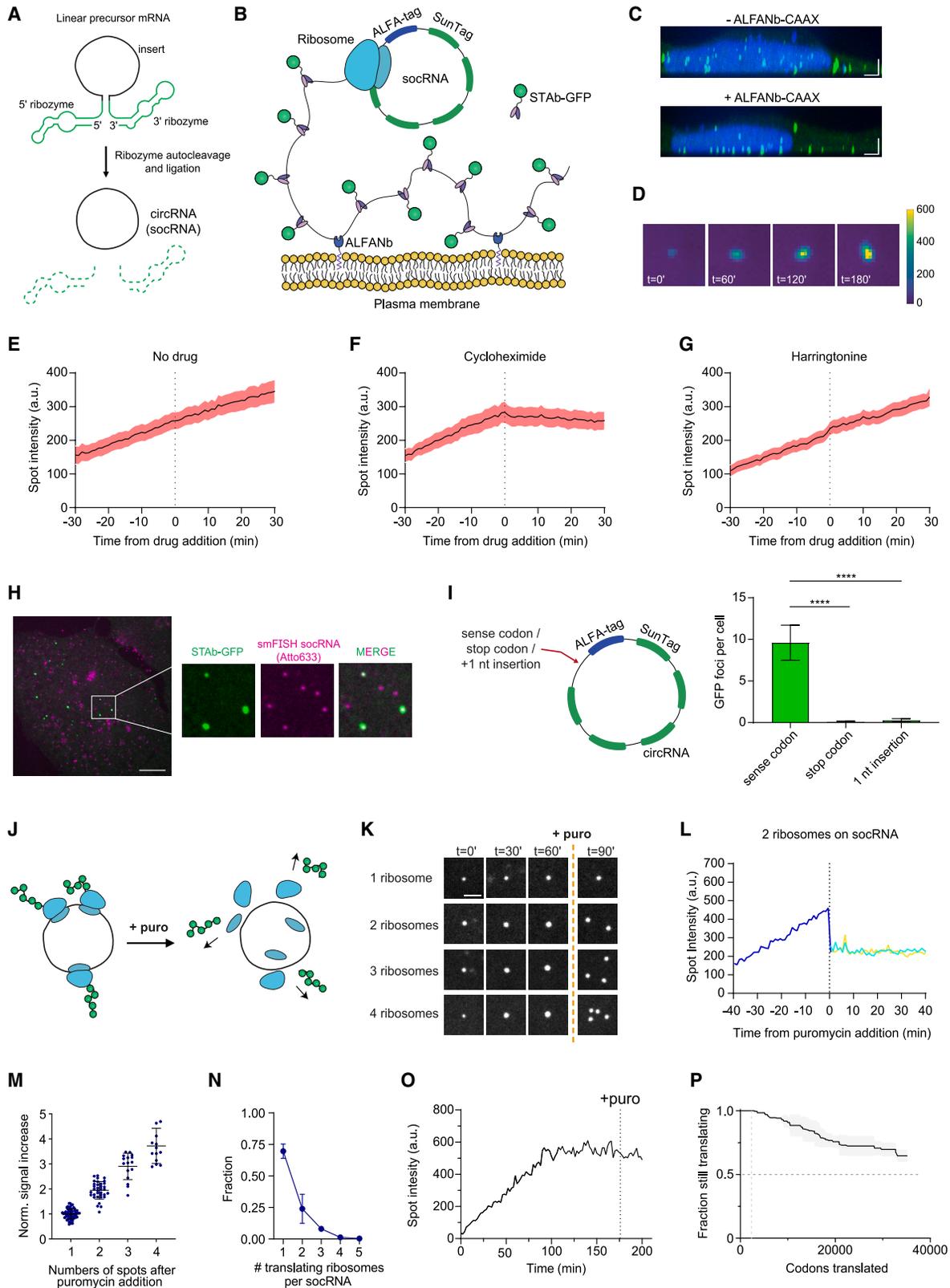
dynamics of translational quality control.[18,19] However, these "first-generation" technologies lack robust single-ribosome resolution, hampering precise kinetic measurements of ribosome-ribosome interactions. Therefore, to study translation elongation kinetics and understand how ribosomes functionally interact, advanced technologies are needed to monitor individual ribosomes with high resolution as they translate an mRNA, both on their own or within polysomes.

RESULTS

Development of socRNAs to study translation elongation dynamics

To measure translation elongation kinetics of single ribosomes, we generated stopless-ORF circular RNAs (socRNAs)—circular RNAs lacking in-frame stop codons (Figures 1A and 1B)—that are translated by one or more ribosomes for hours. SocRNAs allow very precise measurements of translation elongation kinetics and uniquely enable comparisons of translation of the same mRNA sequence by either a single ribosome or multiple ribosomes simultaneously (see below). socRNAs are produced in cells using the Tornado system (Figure 1A),[20] and their translation can be visualized using the SunTag translation imaging system (Figure 1B).[13–17] To enhance imaging and tracking of single socRNAs, we tethered socRNAs to the plasma membrane by encoding a second epitope tag, the ALFA-tag[21] in the socRNA sequence and targeting the cognate ALFA-tag nanobody (ALFANb) to the plasma membrane (Figures 1B and 1C). Finally, we used a doxycycline-inducible promoter for regulated expression of socRNAs. socRNAs were introduced into human U2OS cells expressing both SunTag antibody (STAb)-GFP and membrane-anchored ALFANb and imaged by spinning disk confocal microscopy.

Time-lapse imaging of socRNA-expressing cells revealed GFP foci that increased in intensity over time (Figure 1D; Video S1). Several lines of evidence indicate that these GFP foci represent nascent polypeptides associated with translated socRNAs. First, GFP intensity increase was acutely blocked by the translation

elongation inhibitor cycloheximide (CHX), but not by harringtonine, which only stalls ribosomes on the translation start codon (Figures 1E–1G and S1A). Second, GFP foci that were increasing in intensity co-localized with socRNA smFISH foci (Figures 1H and S1B). Finally, introduction of a stop codon in the SunTag frame, or insertion of one additional nucleotide into the socRNA, which changes the translation frame after completing a full circle of translation, both prevented GFP foci formation (Figure 1I).

To determine the number of ribosomes translating each socRNA molecule, we treated cells with the translation inhibitor puromycin, which releases nascent chains from ribosomes and allows counting of the number of ribosomes that were associated with each socRNA (Figures 1J–1N; Video S2). Puromycin treatment revealed that individual socRNAs were translated by between one and four ribosomes. Control experiments confirmed that multiple ribosomes in individual GFP foci were not translating different socRNAs that co-localized in the cell (Figure S1C). Interestingly, GFP "daughter" foci that formed upon puromycin-induced splitting of GFP foci always showed similar fluorescence intensities (Figures 1L, S1D, and S1E), indicating that all ribosomes on a socRNA had initiated translation at the same time (within minutes of each other), and that no additional ribosomes were loaded on socRNAs at later time points. Consistent with the notion that no additional ribosomes are loaded on socRNAs at later stages, the increase in GFP intensity of individual translated socRNAs, which depends on the number of translating ribosomes (Figure 1M), never increased during the imaging experiment (Figure S1F). Individual ribosomes on socRNAs did occasionally abort translation during imaging, but such events can be readily observed, either as a sudden plateau in the GFP intensity time trace (if the ribosome was translating the socRNA alone) (Figure 1O), or as splitting of GFP foci (if additional ribosomes were translating the same socRNA) (Figure S1G), and such abortive translation events can thus be accounted for in the analysis. In summary, these results show that individual socRNAs can be translated by one or multiple ribosomes, and that addition of puromycin at the end of an experiment provides a straightforward readout of the number of

---

Figure 1. A method for long-term visualization of single translating ribosomes in living cells

(A) Illustration of socRNA formation.

(B) Schematic of socRNA translation imaging system.

(C) Representative images of cells expressing indicated ALFA-tag systems for plasma membrane tethering. Translating socRNAs (green foci) and DNA (blue) are shown.

(D) Fluorescence intensity of a single translated socRNA over time.

(E–G) Average intensities of translating socRNAs over time after addition of indicated drugs. Lines and shaded region indicate mean ± SEM from 2 experiments (7–13 socRNAs per experiment).

(H) Co-localization of socRNAs (smFISH) and their translation signal (STAb-GFP).

(I) Schematic of socRNA (left) and quantification of the number of GFP foci per cell for each socRNA (right) are shown. Error bars are SEM from 2 experiments (13–20 cells per experiment). **** indicates $p < 0.0001$ (t test).

(J and K) Effect of puromycin treatment of socRNA GFP foci. Schematic (J) and representative images of time-lapse movies (K) are shown.

(L) Intensity time trace of a socRNA translated by two ribosomes and treated with puromycin. Light blue and yellow lines represent two daughter foci after splitting that have identical intensities.

(M) Relationship between the number of spots upon puromycin addition and signal increase over time. Horizontal lines and error bars represent mean ± SD.

(N) Distribution of the number of translating ribosomes per socRNA. Mean ± SD from 3 experiments (62–89 socRNAs per experiment).

(O) Representative GFP intensity time trace of a socRNA showing abortive translation before puromycin addition.

(P) Kaplan-Meyer survival curve showing the total number of codons translated by single ribosomes before aborting translation (referred to as processivity). Line and shaded region indicate mean ± SD from 3 experiments (29–85 socRNAs per experiment).

Scale bars: 3 μm in (C), 10 μm in (E), and 2 μm in (K).

See also Figure S1.

ribosomes that had translated each socRNA over the duration of the experiment.

The observation that all ribosomes translating a socRNA molecule initiated translation at the same time prompted us to investigate the mechanisms of translation initiation on socRNAs. We considered two possible mechanisms; first, 43S ribosomes could be slotted directly onto the circular form of the RNA. Alternatively, ribosomes could be loaded on the linear precursor RNA through conventional 5′ cap-dependent loading and scanning, after which ribosomes are "caught" in the socRNA as the RNA circularizes around them (Figure S1H). For translation initiation to occur on linear mRNAs, ribozyme cleavage must occur after nuclear export, at least for a subset of the mRNAs, which would suggest that ribozyme cleavage is relatively slow in cells. To discriminate between these models, we compared socRNA expression from a polIII promoter, which has low levels of mRNA capping,[22] with a polII promoter that has high mRNA capping rates. We found that polII-driven expression of socRNAs resulted in a substantially higher fraction of socRNAs that was translated (Figure S1I), suggesting that translation initiation occurs predominantly on the linear precursor mRNA. Consistent with this idea, the ribosomal load on socRNAs was strongly increased upon introduction of an AUG translation start codon in the 5′ UTR of the linear precursor RNA, a sequence that is not present in the circular RNA (Figures S1J and S1K), confirming that initiation mostly occurs on the linear precursor mRNA. Moreover, the reading frame of the 5′ AUG largely determined the reading frame of ribosomes translating the socRNA (Figures S1L–S1N). These results show that most ribosomes initiate translation on the linear precursor mRNA and are caught in the socRNA upon circularization. Initiation on linear precursor mRNAs allows modulation of the ribosomal load on socRNAs without altering the socRNA coding sequence by changing the 5′ UTR sequence. We note that a small fraction of ribosomes (~20%) translated the socRNA in a reading frame that differed from the 5′ AUG reading frame (Figure S1N). These ribosomes may have initiated at non-canonical translation initiation codons during scanning or may have initiated on linear mRNAs through an alternative mechanism.

Having established socRNAs as a robust and reliable assay to visualize translation of single or multiple ribosomes, we asked whether socRNAs could be used to precisely measure ribosome translocation dynamics. GFP intensities of nascent polypeptides associated with socRNAs were measured over time and translation elongation rates were calculated based on the slope of GFP intensities over time (see STAR Methods). These measurements revealed a mean elongation rate of 2.6 codons/s, very similar to our previous measurements on linear mRNAs in the same cells.[14] Importantly, membrane tethering of socRNAs did not detectably affect elongation rates (Figure S1O) (see STAR Methods). We also introduced known pause sequences into the socRNA and confirmed that socRNAs accurately recapitulate pausing on these sequences and allow very precise quantification of pause duration (Figures S1P and S1Q). In addition to measurements of translation elongation rates, the socRNA assay also uniquely allows measurements of ribosome processivity (defined as the total number of codons translated until a ribosome aborts translation), a parameter that is difficult to access using conventional assays. Ribosome processivity reports on a number of different processes, including (1) translation termination on sense codons, (2) ribosome recycling in the absence of termination—such as through activation of quality control mechanisms, (3) ribosome frameshifting followed by termination on a stop codon in the alternative reading frame, or (4) socRNA decay. Analysis of ribosome processivity on control socRNAs showed that ribosomes are highly processive, translating on average ~70,000 codons before aborting translation (Figures 1O and 1P). Together, these results show that socRNAs allow precise measurements of translation elongation dynamics, and, as such, provide a powerful tool to study the translation elongation phase.

Translation elongation rates of individual ribosomes

To understand how the activity of ribosomes is coordinated on a RNA, it is critical to know the translocation dynamics of individual ribosomes. A number of studies have shown that ribosomes can vary in composition and that such compositional heterogeneity may be functionally relevant for different aspects of translation.[23,24] To assess possible heterogeneity in translocation dynamics, we precisely measured translocation rates of individual ribosomes using socRNAs. Interestingly, when measuring GFP foci intensity over time for socRNAs translated by single ribosomes, we found that rates of GFP increase varied considerably between different ribosomes (Figure 2A), suggesting that different ribosomes move at distinct speeds. To control for technical noise in these measurements that could account of heterogeneity in the slope of GFP intensity time traces, we also examined intensity time traces of GFP foci that did not increase in intensity over time ("plateau traces," which represent polypeptides for which translation was aborted), which likely have similar technical noise. To compare plateau traces with "increasing traces," we transformed the slope of plateau traces with a fixed value, equal to the average slope of increasing traces (Figure 2B). While plateau traces did show some heterogeneity in their slopes as well, the heterogeneity was substantially smaller than that of increasing traces (Figure 2C), demonstrating that technical noise alone cannot explain the heterogeneity in translation elongation rates. An independent mathematical approach confirmed that the expected heterogeneity in translation elongation rates from technical noise and stochastic translocation is not sufficient to explain the observed heterogeneity in elongation rates (Figures 2D and S2A–S2E; see STAR Methods). Observed elongation rate heterogeneity could also not be explained by cell-to-cell differences in expression of the STAb-GFP (Figure S2F), nor by sequence variations of socRNAs (Figure S2G). We further examined socRNA mobility as a proxy for organelle/membrane association (e.g., ER-localized translation) but found no significant correlation between socRNA mobility and translation elongation rate (Figure S2H). Nascent chain length also did not correlate with elongation speed (Figures S2I and S2J). Finally, neither stochastic pauses in translation elongation, nor cell-to-cell heterogeneity in elongations rates could explain the apparent elongation heterogeneity between ribosomes (Figures S2K–S2O; see STAR Methods). Together, these findings are most consistent with a model in which intrinsic ribosome heterogeneity explains the elongation speed heterogeneity, although our results cannot completely exclude that elongation
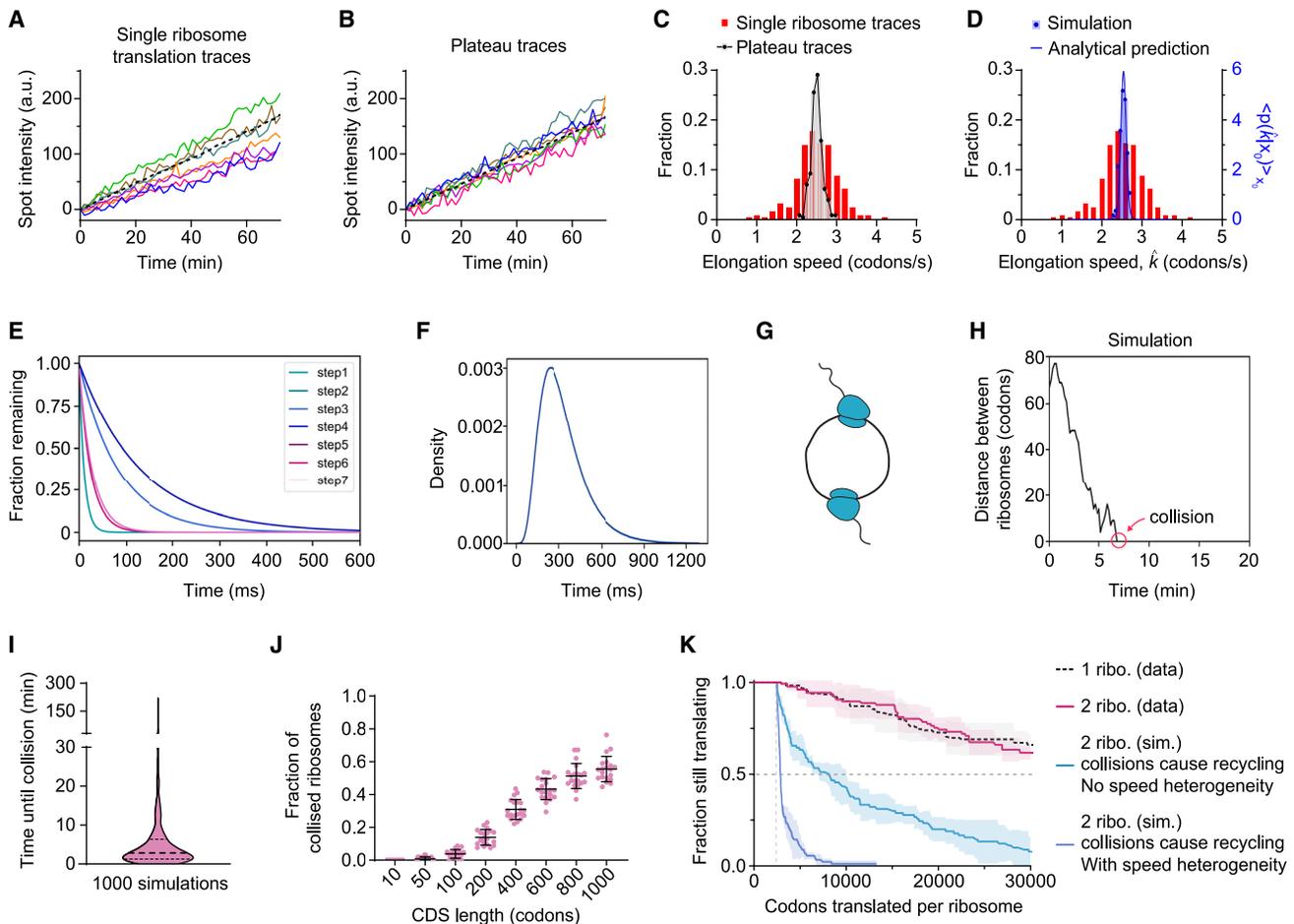
Figure 2. Transient collisions between translating ribosomes do not induce ribosome recycling

(A–D) Representative intensity time traces (A and B) and two types of quantification (C and D; see STAR Methods) of single ribosomes translating socRNAs (A) or transformed plateau traces that indicated technical noise (B; see STAR Methods). Starting intensities were set to 0. Black dashed lines indicate mean from 142 (A) or 227 (B) socRNA traces (n = 3 experiments).

(E and F) Distributions of the duration of each step (E) or the complete translation elongation cycle (F) used in simulations.

(G) Schematic depicting socRNA simultaneously translated by two ribosomes.

(H and I) Simulation of the time until the first collision between two ribosomes translating the same socRNA. Representative example (H) and quantification of 1,000 simulations (I) are shown.

(J) Simulation of ribosome collisions on linear mRNAs (see STAR Methods). Each dot represents a single mRNA. Horizontal lines and error bars represent mean ± SD.

(K) Kaplan-Meyer survival curve showing the total number of codons translated before aborting translation of experiments (data) and simulations (sim.). Dashed black line is replotted from Figure 1P. Lines and shaded regions indicate mean ± SD from 3 experiments (24–54 ribosomes per experiment).

See also Figures S2 and S3.

speed heterogeneity is caused by non-sequence differences between socRNAs (e.g., nucleotide modifications or RNA damage).

Transient ribosome collisions do not result in ribosome recycling

An intriguing consequence of elongation speed heterogeneity is that different ribosomes translating the same socRNA could undergo frequent collisions during translation. To quantify collision frequency between translating ribosomes and to explore the role of ribosome elongation speed heterogeneity in such collisions, we used stochastic computer simulations of translation elongation dynamics (see STAR Methods; Figures 2E–2I). To validate

our simulations, we first simulated elongation dynamics of single ribosomes and determined the elongation rate distribution of many single ribosomes, which resulted in a very similar distribution as was observed experimentally (Figure S3A). Interestingly, simulation of socRNA translation by two ribosomes revealed that translocating ribosomes rapidly collided on socRNAs, with a median time to collision of just ~3 min (Figures 2G–2I). The occurrence of collisions was very robust to variations in simulation parameters (Figures S3B–S3D), confirming the validity of these results. Even when ribosome elongation speed heterogeneity was excluded from simulations, collisions between translating ribosomes occurred frequently on socRNAs under all tested
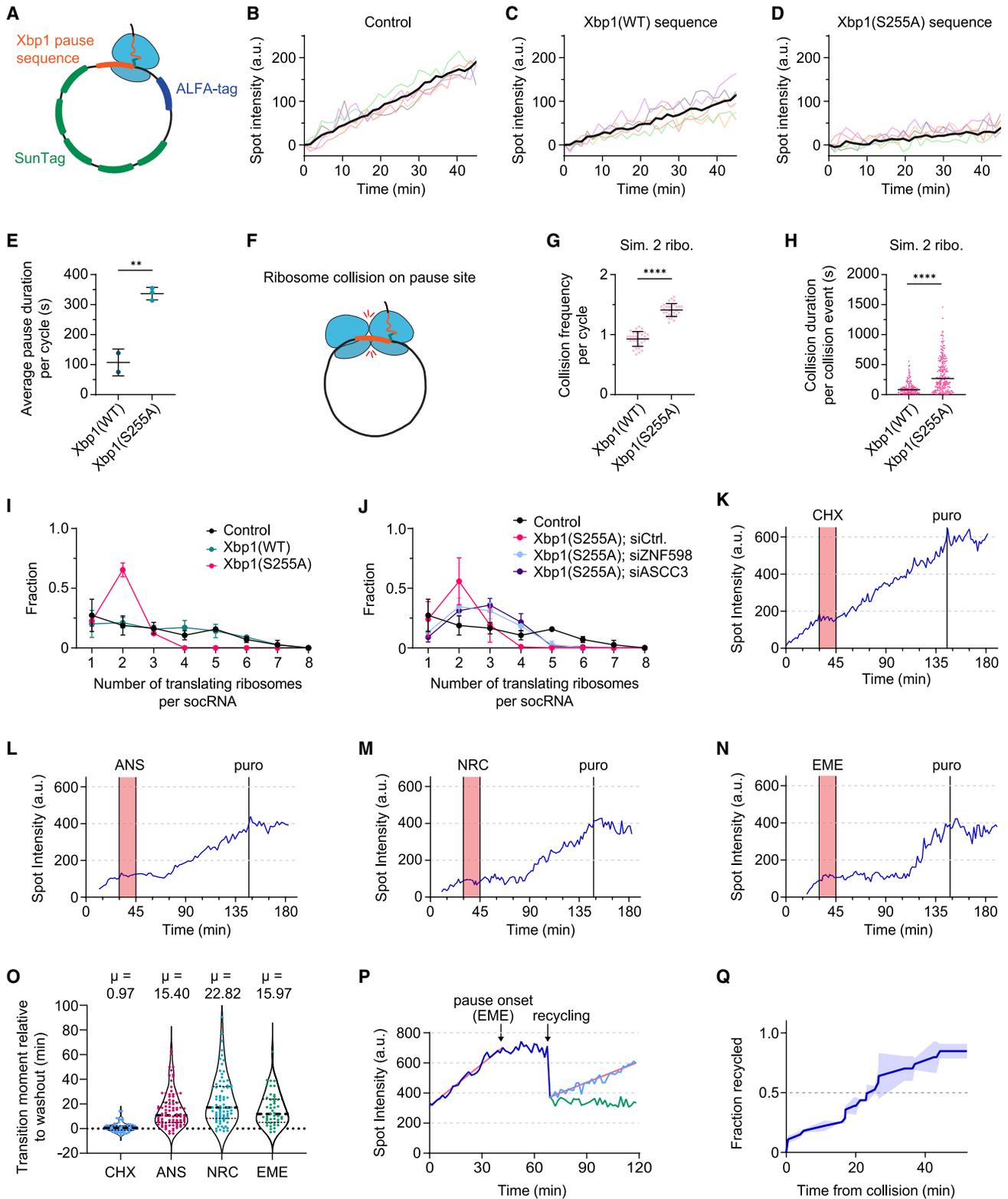
Figure 3. Ribosome collision duration and queue length determine recycling efficiency

(A) Schematic of socRNA with Xbp1 pause sequence.

(B–E) Representative intensity time traces (B–D) and average pause durations (E; see STAR Methods) of single ribosomes translating indicated socRNAs.

(B–D) Black line indicates mean values.

parameters due to the stochastic nature of translation elongation, albeit with somewhat delayed kinetics (Figure S3E). Additional simulations revealed that ribosome collisions are also frequent on linear mRNAs (Figures 2J and S3F–S3I; Videos S3 and S4). Collectively, these simulations indicated that collisions between translating ribosomes regularly occur on both socRNAs and linear mRNAs.

We next asked whether collisions between two translating ribosomes cause ribosome recycling. If so, ribosome processivity should be much lower when a socRNA is translated by two ribosomes or more ribosomes compared with socRNA translated by one ribosome, given the high frequency of collisions on socRNAs identified in our simulations. However, we found that ribosome processivity is not affected by the number of ribosomes translating a socRNA (Figures 2K and S3J), indicating that transient collisions between translating ribosomes do not result in ribosome recycling. We wondered how cells could discriminate such transient, "physiological" collisions from persistent, "pathological" collisions to ensure that only the latter type is recycled by surveillance mechanisms. One possibility is that physiological collisions are too short lived for quality control pathways to target them. While we can estimate the lifetime of physiological collisions to be on the milliseconds-to-seconds timescale (the time a ribosome typically spends on a single codon), the time needed for surveillance mechanisms to identify and recycle collided ribosomes is unknown. Therefore, we set out to determine the kinetics of ribosome collision sensing and recycling. To generate long-lived ribosome collisions, we used the well-studied pause sequence of the Xbp1 mRNA (referred to as Xbp1 socRNAs) (Figure 3A), which pauses ribosomes at a well-defined site due to inhibition of peptide bond formation.[25,26] We also included a mutant of Xbp1 (S255A) that shows increased pause strength.[26] Comparing control with Xbp1 and Xbp1(S255A) socRNAs translated by single ribosomes allowed precise quantification of pause durations (107 ± 45 s and 337 ± 21 s on the Xbp1[WT] and Xbp1[S255A] sequences, respectively) (Figures 3B–3E). Since the average pause duration on the Xbp1 socRNAs is similar to or longer than the average time needed for a ribosome to translate the remainder of the socRNA, collisions are expected to occur frequently on both Xbp1 socRNAs, which we confirmed through simulations (Figures 3F–3H). As expected, both collision frequency and duration were higher for Xbp1(S255A) than Xbp1(WT) socRNAs (Figures 3G and 3H). If collisions between

a translating and a paused ribosome on Xbp1 socRNAs cause ribosome recycling, the average ribosomal load per socRNA should progressively decrease over time (since ribosomes are exclusively loaded on socRNAs at the start of the experiment) (Figures S1D and S1E). Therefore, high ribosomal load socRNAs (see Figure S1K) were used for these experiments to assess recycling efficiency. When analyzing ribosome number per socRNA after 10 full cycles of translation, the number of ribosomes per socRNA was strongly reduced for Xbp1(S255A) socRNAs compared with control socRNAs (Figure 3I; see STAR Methods). This reduction in ribosome number was rescued by knockdown of ZNF598 or ASCC3 (Figures 3J, S4A, and S4B), proteins involved in recycling of collided ribosomes,[11,27,28] confirming that the reduced ribosome number was caused by collision-induced ribosome recycling. Surprisingly though, while Xbp1(S255A) socRNAs showed a substantial drop in the number of translating ribosomes per socRNA, the number of ribosomes on Xbp1(WT) socRNAs was indistinguishable from control reporters, even though our simulations show that collisions between a paused and a translocating ribosome occur frequently on Xbp1(WT) socRNAs as well, albeit with shorter durations (Figures 3G and 3H). These results confirm that relatively brief collisions between paused and translocating ribosomes are not targeted for ribosome recycling, but when collisions persist for longer periods of time (as is the case for the Xbp1[S255A] pause site), ZNF598 and ASCC3 have sufficient time to sense such collisions and target them for recycling.

To confirm through an independent method that prolonged collision duration is essential for efficient recycling of collided ribosomes, we aimed to acutely induce ribosome collision using a low dose of a translation elongation inhibitors and measure the time from collision to recycling. For this assay it is important that single inhibitor molecule binding events result in ribosome pauses that are long enough for ribosome collisions and recycling to occur. While many different translation elongation inhibitors have been described,[29,30] the ribosome dissociation kinetics of these inhibitors in vivo are largely unknown. We therefore first assessed dissociation kinetics of various elongation inhibitors—CHX, anisomycin, emetine, and narciclasine—to identify an inhibitor that could be used for our experiments. At high concentrations, all four drugs completely inhibited translation elongation, as expected (Figure S4C). When drugs were washed out (Figure S4D), translation rapidly (<1 min) resumed

---

(E) Mean ± SD from 2–3 experiments are shown (23–56 socRNAs per experiment).

(F–H) Simulation of ribosome collision on socRNA with Xbp1 pause site.

(G) Collision frequency per cycle at the Xbp1 pause site from simulations (see STAR Methods). Note that a ribosome can collide twice during one cycle of translation (once as the leading and once as the trailing ribosome). Dots represent individual simulations. Horizontal lines and error bars indicate mean ± SD.

(H) Collision durations from simulations for indicated socRNAs. Each dot represents one collision event. Horizontal lines indicate median.

(I and J) Distributions of the number of translating ribosomes per socRNA. Mean ± SD of 2–3 experiments is shown (12–66 socRNAs per experiment).

(K–N) Representative intensity time traces of single ribosomes translating socRNAs treated with indicated ribosome-targeting drugs.

(O) The time from drug removal to resumption of translation. Dashed lines indicate median, thin lines indicate 25th and 75th percentile (n = 2 experiments, 18–47 ribosomes per experiment).

(P and Q) Low dose of emetine (EME, 33 ng/mL) was added to cells expressing a control socRNA at t = 30 min to induce ribosome collisions, and the moment of ribosome recycling (GFP foci splitting) was determined. Representative intensity time trace (P) and quantification (Q) are shown. Red lines in (P) show linear fits. The slope of the second red line is about half the slope of the first line, indicating that the number of translating ribosomes is reduced by half. Lines and shaded regions in (Q) indicate mean ± SD from 2 experiments (12–16 socRNAs per experiment).

** and **** indicate $p < 0.01$ and 0.0001 (t test), respectively.

See also Figure S4.

for CHX (Figure 3K), demonstrating that CHX dissociates very rapidly from stalled ribosomes. In contrast, anisomycin, emetine, and narciclasine all induced long-lived ribosome stalls after drug washout (>10 min) (Figures 3L–3O and S4E; see STAR Methods), demonstrating that they have low off-rates *in vivo*. These results reveal the *in vivo* dynamics of commonly used ribosome-targeting drugs and identify anisomycin, emetine, and narciclasine as useful tools to induce ribosome collisions in our assay.

To determine the kinetics of ribosome recycling upon collision, we treated cells with a low dose of emetine during socRNA imaging to pause at most one ribosome per socRNA (Figure S4F). To prevent overloading of the cell-wide ribosome collision surveillance pathway, harringtonine was added to cells 30 min prior to emetine addition to induce run-off of ribosomes on endogenous mRNAs. Emetine-induced ribosome collision and recycling could be readily identified on socRNAs translated by multiple ribosomes as sudden transitions in GFP intensity time traces from signal increase to plateau, followed by GFP foci splitting (Figure 3P). Quantitative analysis revealed that ribosome recycling upon collision was slow, with a median time of 22 min (Figure 3Q; see STAR Methods). Thus, collision-induced ribosome recycling is slow compared with the duration of transient ribosome collisions. Slow sensing and recycling of collisions likely underlies the selective recycling of pathological over physiological collisions.

When examining ribosomal load on Xbp1(S255A) socRNAs, we noticed that the number of socRNAs with *three or more* ribosomes was strongly reduced compared with control socRNAs, but the number of socRNAs with *two* ribosomes was not (Figure 3I). If collisions between two ribosomes would result in effective ribosome recycling, only a single ribosome should remain on Xbp1(S255A) socRNAs. Thus, these results suggest that collisions between three or more ribosomes may cause more efficient ribosome recycling than collisions between two ribosomes. Collisions between two ribosomes may not be entirely immune to collision-induced recycling though, as we observed a slight increase in processivity for Xbp1(S255A) socRNAs translated by two ribosomes upon depletion of ZNF598 by siRNA (Figure S4I). In summary, these results suggest that collision duration and queue length together shape recycling efficiency. Because collisions caused by a stalled ribosome result in substantially longer durations and queue lengths compared with collisions between two translocating ribosomes, these findings offer a plausible explanation for the effective discrimination between physiological and pathological collisions.

Ribosome cooperativity drives fast and efficient translation

Since transient collisions do not appear to induce ribosome recycling, we wondered whether such transient collisions might affect ribosome translocation in other ways. Simulating translation of socRNAs by either one or two ribosomes revealed that ribosomes move slightly slower when translating the socRNA together (Figure 4A), an effect we term "ribosome interference." Such ribosome interference is expected as a result of heterogeneous ribosome translocation rates (both due to the stochastic nature of translocation and elongation speed heterogeneity) and the inability of a faster ribosome to overtake the slower

one. Ribosome interference was minimal when both ribosomes were continuously translocating but became more pronounced when a pause site was introduced into a socRNA because a paused ribosome creates a long-lived block of translocation for the trailing ribosome (Figure 4B; Video S5). To test for ribosome interference experimentally, we focused on socRNAs containing the Xbp1(S255A) pause site, as the effect of ribosome interference in the absence of pause sites is likely too subtle to detect experimentally. Surprisingly, when comparing elongation rates of two ribosomes versus one, two ribosomes together translated the Xbp1(S255A) socRNA substantially faster than expected based on simulations (Figures 4C and 4D), and even faster than single ribosomes translating the same sequence (Figures 4C and 4D). Increased translation rates for two ribosomes compared with one was specific for pause sequences, as control socRNAs lacking pause sequences were translated at similar rates by one or two ribosomes (Figures 1M and 4A). These results indicate that the second ribosome specifically reduces pausing of the first ribosome on the pause site. The pause duration for socRNAs translated by three ribosomes was similar to socRNAs with two ribosomes, indicating that two ribosomes are sufficient to maximally reduce pause duration (Figure S5A). These results reveal that ribosomes can help each other overcome strong pauses, a mechanism we term "ribosome cooperativity."

We wondered whether ribosome cooperativity also acts on other types of translational pauses. To investigate this, we first assessed the pause time on socRNAs encoding a stretch of 8xAAA lysine codons, which is known to slow down ribosome translocation both due to the homopolymeric stretch of adenosines and the positively charged nascent chain.[31] Poly(A) sequences can also induce ribosome frameshifting,[31] but frameshifting is not expected to interfere with translation elongation rate measurements on socRNAs, since ribosomes will rapidly terminate translation on stop codons in alternative reading frames upon frameshifting. Similar to the Xbp1(S255A) socRNAs, the average pause duration for two ribosomes translating $(AAA)_8$ socRNAs was substantially shorter than that of single ribosomes translating the same sequence (Figures 4E and 4F). Finally, we also examined socRNAs containing an RNA pseudoknot, a strong RNA structure,[32] which we found acts as a potent pause site for translocating ribosomes (Figures 4G and 4H). Similar to Xbp1(S255A) and poly(A) sequences, two ribosomes translating an RNA pseudoknot containing socRNA pause shorter than single ribosomes (Figures 4G and 4H). Reduction of the average pause duration on RNA structures may have an additional explanation; if two ribosomes are queued upstream of a RNA structure and the first ribosome has successfully unfolded the structure and resumes translation, the trailing ribosome will follow closely, preventing the structure from reforming in between the two ribosomes. In this scenario, the trailing ribosome is not impeded by the RNA structure when the structure is unfolded by the leading ribosome, somewhat analogous to a "slipstream" effect (Figure 4I). To test whether the slipstream effect is sufficient to quantitatively explain the shorter pause times for two versus one ribosome on pseudoknot socRNAs, we included the slipstream effect in our simulations. While the slipstream effect reduced the average pause time
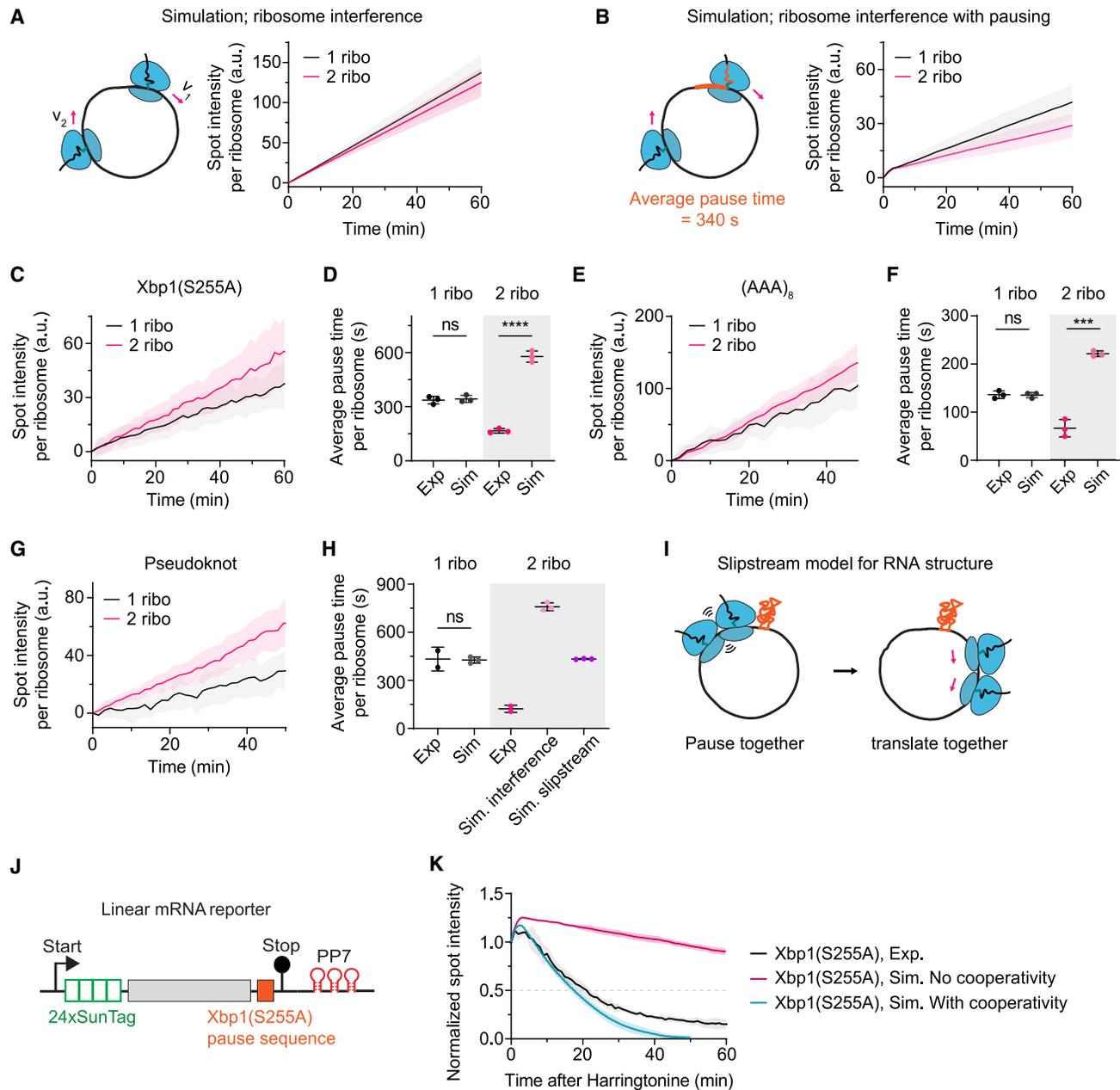
Figure 4. Ribosome cooperativity reduces ribosome pausing

(A and B) Simulation of GFP intensity of socRNA translation foci for socRNAs with (A) or without (B) pause site (see STAR Methods).

(C–H) U2OS cells stably expressing STAb-GFP, ALFANb-CAAX, and Tet repressor (TetR) were transfected with indicated socRNAs and imaged by time-lapse microscopy.

(C, E, and G) Average intensity time traces of socRNA translation foci for indicated socRNAs. Lines and shaded regions indicate means ± SD.

(D, F, and H) Pause time per ribosome per full cycle of translation for experiments and simulations. Total pause time includes pause time at pause site and "waiting time" when trailing ribosome is paused upstream of a ribosome paused at the pause sequence. Dots represent average data from individual experiments or simulations. Mean ± SD of experiments or simulations is shown.

(C and D) Xbp1(S255A) (*n* = 3 experiments, number of socRNAs: 1 ribo = 85, 2 ribo = 39).

(E and F) (AAA)$_8$ (*n* = 3 experiments, number of socRNAs: 1 ribo = 11, 2 ribo = 23).

(G and H) RNA pseudoknot (*n* = 2 experiments, number of socRNAs: 1 ribo = 16, 2 ribo = 13).

(I) Cartoon illustrating the slipstream model of ribosome translation of mRNA structures.

(J) Schematic depicting the linear mRNA translation reporter used in (K).

(legend continued on next page)

per ribosome for socRNAs translated by two ribosomes, as expected, comparison of simulations with experiments showed that two ribosomes still moved substantially faster than expected, even when the slipstream effect was included in simulations (Figure 4H). These results show that the trailing ribosome must also suppresses pause duration of the *leading* ribosome paused upstream of a RNA structure, possibly by cooperating to unfold the RNA structure. Finally, we asked whether drug-induced ribosome pauses could also be reduced by ribosome cooperativity. To this end, we treated cells with inhibitors of ribosome translocation (emetine) or peptide bond formation (anisomycin and narciclasine) and compared elongation rates for socRNAs translated by one or two ribosomes. In this assay, a lower average elongation rate is expected for socRNAs translated by two ribosomes compared with one, since each ribosome on the socRNA can bind the drug independently, and drug binding to any one of the ribosomes on the socRNA results in translational pausing of all ribosomes on the socRNA. Indeed, for low-dose emetine treatment, average translation rates per ribosome are substantially reduced for socRNAs translated by two as compared with one ribosome (Figures S5B and S5C), indicating that ribosome cooperativity does not act on emetine-bound ribosomes. However, for both anisomycin and narciclasine, translation rates for socRNAs translated by two ribosomes were higher than those for socRNAs with one ribosome, indicative of ribosome cooperativity (Figures S5D and S5E). Together, these results show that ribosome cooperativity helps resolve diverse translational pauses.

To validate that ribosome cooperativity also acts in the context of linear mRNAs, we assessed pause duration on linear mRNAs encoding a Xbp1(S255A) pause sequence using harringtonine-induced ribosome run-off. A complicating factor in these experiments is that apparent harringtonine run-off rates are not only affected by translation elongates rates and pause durations but also by collision-induced ribosome recycling. To eliminate collision-induced ribosome recycling as a complicating factor, experiments were performed in ZNF598 knockout cells (Figure S5F). We first confirmed that ZNF598 knockout did not alter pause duration on the Xbp1(S255A) pause site (Figure S5G). We then performed simulations of ribosome run-off, either with or without ribosome cooperativity (Figure 4K; see STAR Methods). Comparing experiments with simulations revealed that experimental run-off values closely match simulations with ribosome cooperativity (Figure 4K), strongly suggesting that ribosome cooperativity also occurs on linear mRNAs. We note that a subset of ribosomes (~15%) showed slow run-off in our experiments, which was not captured in our simulations (Figure 4K, right tail). Slow run-off in experimental data may be caused by ribosomes that are naturally stalled on mRNAs *in vivo*, possibly due to damaged mRNA, consistent with our previous ribosome run-off experiments.[14]

To determine whether ribosome collisions are needed for ribosome cooperativity to reduce pause duration, we simulated socRNA translation dynamics assuming that collisions instantaneously resolve pausing of the leading ribosome upon collision (Figures 5A and 5B; Video S6). For both the Xbp1(S255A) and the poly(A) reporter, these simulations showed that collision-induced pause resolution explains the reduction in pause duration relatively well (Figures 5A and 5B). However, the experimentally determined pause durations were slightly higher than the simulation results, suggesting that ribosome cooperativity does not always occur instantaneously upon collision. Addition of either a small delay (~15–40 s) between collision and resumption of translation or including the assumption that a small subset of collision events does not successfully resolve pausing, allowed quantitative matching of simulations and experiments (Figures S6A–S6D). To experimentally validate that ribosome collisions underlie ribosome cooperativity, we designed socRNAs with two Xbp1(S255A) pause sites per socRNA (Figure 5C), which show reduced ribosome collision frequency in our simulations (Figure 5D). Indeed, ribosome cooperativity was reduced by reduction of collisions, and the magnitude of this reduction closely matched our simulations which assumed that collisions underlie suppression of pause duration (Figure 5E). Similarly, introduction of multiple shorter poly(A) pause sites reduced collision frequency, without affecting total pause duration per translation cycle. SocRNAs with multiple poly(A) sequences also showed a reduction in ribosome cooperativity, consistent with our simulations (Figures 5F–5H). Together, these results strongly suggest that collisions drive ribosome cooperativity by suppressing ribosome pausing at problematic sequences.

We next asked whether ribosome cooperativity also altered translation processivity. Introduction of either a Xbp1(S255A) sequence, a pseudoknot RNA structure or a poly(A) sequence reduced processivity to varying degrees when socRNAs were translated by one ribosome (Figures S7A–S7C). However, ribosome processivity was largely rescued when socRNAs were translated by two or more ribosomes (Figures 6A–6C and S7D–S7G). Thus, we conclude that ribosome cooperativity can enhance both translation speed and processivity. To understand how ribosome cooperativity enhances translation processivity, it is important to understand what causes reduced processivity of single ribosomes translating a pause sequence, as ribosome cooperativity likely suppresses this cause. A recent study in yeast suggested that single stalled ribosomes, like collided ribosomes, may be recycled by surveillance mechanisms,[33] but a pathway targeting single ribosomes has not yet been identified in human cells. SocRNAs translated by single ribosomes offer a unique opportunity to assess recycling of paused ribosomes in the absence of ribosome collisions. To determine whether the decreased processivity of single ribosomes on socRNAs with pause sites was caused by ribosome surveillance mechanisms, we depleted the helicase ASCC3, the downstream effector of the ribosome recycling pathway.[27,34] When examining ribosome processivity on the poly(A) socRNA,

(K) Ribosome run-off by harringtonine on linear reporter shown in (J). Experiments (Exp.) and simulations (Sim.) with or without ribosome cooperativity are shown (see STAR Methods).

*** and **** indicate $p < 0.001$ and 0.0001 (t test), respectively.

See also Figure S5.

Cell
Article
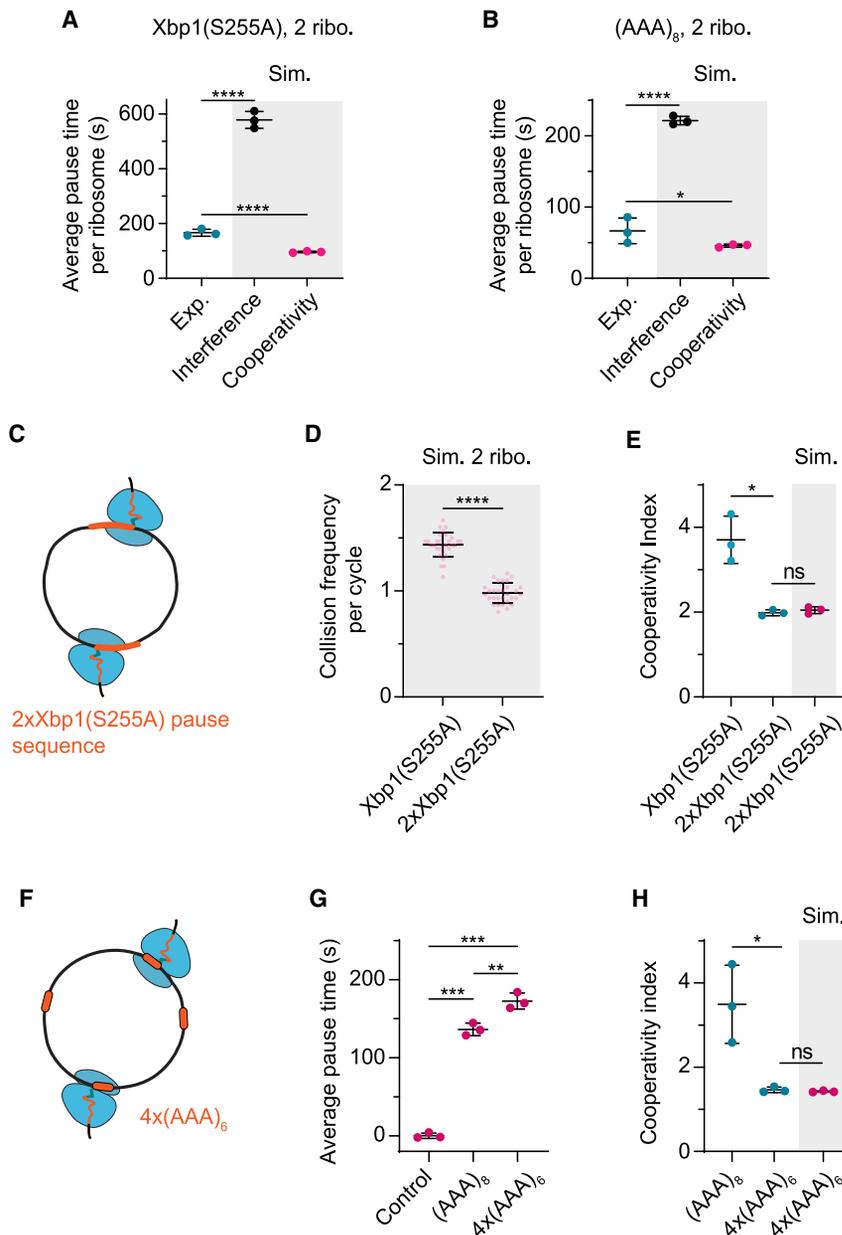
Figure 5. Evidence that collisions underlie ribosome cooperativity

(A and B) Average pause time per full cycle of translation on indicated socRNAs translated by two ribosomes for experiments (Exp.) and simulations (Sim.) using different models. Cooperativity model used for simulations assumes that ribosomes immediately resume translation upon collision. Cyan and black dots are replotted from Figures 4D and 4F for comparison.

(C) Schematics depicting socRNA containing 2xXbp1(S255A) pause sequences.

(D) Simulation of collision frequency per full cycle of translation. Values higher than 1 indicated that ribosomes (occasionally) collided twice per cycle, once as the leading and once as the trailing ribosome. Collision events *per pause site* were calculated for 2xXbp1(S255A) socRNA to make the data comparable to the 1xXbp1(S255A) socRNA.

(E) The cooperativity index for socRNAs containing either one or two Xbp1(S255A) pause sequences was calculated from simulations (magenta) and experiments (cyan) (see STAR Methods) ($n = 3$ experiments, 5–23 socRNAs per experiment). The cooperativity index is defined as the pause time expected from the ribosome interference simulation divided by the experimentally determined pause time (see STAR Methods).

(F) Schematics depicting socRNA containing 4x(AAA)$_6$ pause sequences.

(G) The average total pause duration per full cycle of translation is shown for indicated socRNAs ($n = 3$ experiments, 11–21 socRNAs per experiment).

(H) The cooperativity index for socRNAs containing a single (AAA)$_8$ ($n = 3$ experiments, 5–18 socRNAs per experiment) or four (AAA)$_6$ ($n = 3$ experiments, 11–19 socRNAs per experiment) was calculated from experiments (cyan) or simulations (magenta).
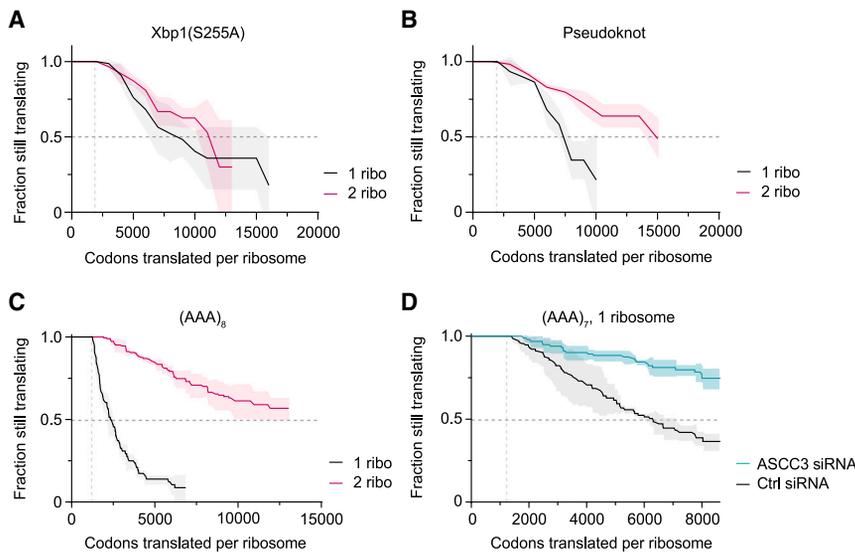
*, **, ***, and **** indicate $p < 0.05$, 0.01, 0.001, and 0.0001 (t test), respectively. Horizontal lines and error bars represent mean ± SD. Dots represent data from independent experiments or simulations.

See also Figure S6.

we found that processivity of single ribosomes was strongly enhanced upon depletion of ASCC3 (Figure 6D). These results reveal that a ribosome surveillance pathway targets single, paused ribosomes in human cells, and suggest that ribosome cooperativity enhances processivity by suppressing this surveillance pathway.

Finally, we tested whether ribosome cooperativity also enhances translation of "normal" mRNA sequences (i.e., those that do not encode pause sequences). We observed occasional long-lived pauses in single-ribosome intensity time traces on normal mRNA sequences (Figures 7A and 7B; see STAR Methods), so we assessed whether ribosome cooperativity also helps to overcome such stochastic pauses. Using a strin-

gent cutoff for pause detection, we could identify prolonged pauses in ~5% of intensity time traces of socRNAs translated by single ribosomes (mean pause time ~10 min). We next examined ribosome pausing for socRNAs translated by two or more ribosomes. A higher fraction of socRNAs is expected to show pausing for socRNAs translated by multiple ribosomes, as a stochastic pause of any one of the ribosomes blocks elongation of all ribosomes on the socRNA. However, rather than an increase, we observed a stark reduction in pause frequency on socRNAs translated by two or more ribosomes (Figure 7C), indicating that ribosome cooperativity suppresses stochastic ribosome pausing as well. The absence of detectable pauses for socRNAs translated by multiple ribosomes was not due to recycling of

Figure 6. Ribosome cooperativity enhances processivity by limiting ribosome recycling

(A–D) Kaplan-Meyer survival curves of indicated socRNAs show the total number of codons translated by ribosomes before aborting translation. Lines and shaded regions indicate mean ± SD from 2–3 experiments (5–42 socRNAs per experiment). See also Figure S7.

ribosome ubiquitination upon collision might be the rate-limiting step in recycling (minutes), while splitting of ubiquitinated ribosomes is fast (seconds). In long steady-state queues, ribosomes may have had sufficient time to become ubiquitinated, so the observed recycling kinetics under those conditions are driven mainly by the fast ribosome splitting rates. In contrast, in our socRNA assay, the time from initial collision to recycling is assessed, which includes both the time for ubiquitination and ribosome splitting, resulting in far slower measured recycling times. Our work also provided evidence that recycling efficiency is dependent on ribosome queue length as well (Figure 3). Consistently, a recent in vitro study has shown that ubiquitination of collided ribosomes occurs more efficiently for longer ribosome queues.[34] Longer ribosome queues may increase the total time a ribosome spends in a collided state, thus enhancing ubiquitination. More speculatively, longer queues of collided ribosomes could also increase ubiquitination rates, for example, by increasing local concentration of surveillance proteins near collided ribosomes. Combined, our results suggest a unifying model for ribosome collisions: transient, physiological ribosome collisions do not induce ribosome recycling and can even relieve ribosome pausing through cooperativity, but if ribosome pausing persists after collision, long and stable ribosome queues will form, resulting in efficient recycling of the stalled ribosome. Future work will be aimed at measurements of recycling kinetics in different cell types with varying expression levels of recycling factors, as well as measurements of collision-induced recycling rates at different types of pause sequences.

paused ribosomes upon collisions, as we observed a similar low pause frequency of socRNAs translated by multiple ribosomes after ASCC3 knockdown (Figure 7D). Suppression of stochastic ribosome pausing by multiple ribosomes may offset translation slowdown caused by ribosome interference, possibly explaining why two ribosomes move at similar rates as single ribosomes on control socRNAs. In summary, these results show that ribosome cooperativity acts to suppress stochastic pausing of ribosomes on normal mRNA sequences, which may reflect the function of ribosome cooperativity in cells.

DISCUSSION

In this study, we developed socRNAs, a broadly applicable technology to measure translation elongation rates of individual ribosomes in living cells. The socRNA assay allows high precision measurements of translation elongation rates, comparison of translation by one versus multiple ribosomes and allows measurements of ribosome processivity. Employing the socRNA assay in combination with computer simulations, we found that transient ribosome collisions reduce ribosome pausing and promote processive translation through a process we term ribosome cooperativity. This work suggests that the high ribosome load on mRNAs typically observed during eukaryotic translation might enhance translational efficiency through ribosome cooperativity.

### Discriminating between physiological and pathological collisions

In this study, we provide evidence that transient collisions occur frequently but are not sensed by ribosome surveillance mechanisms. We show that sensing and recycling of ribosome collisions is slow (minutes timescale) relative to the duration of transient collisions (milliseconds-seconds timescale). Our results on recycling kinetics appear to contrast a recent study which found that ribosomes in long steady-state queues are recycled within seconds.[18] One possible explanation for this discrepancy is that

Possible mechanisms underlying ribosome cooperativity

Our simulations suggest at least three, non-mutually exclusive mechanisms underlying ribosome cooperativity, which may act to resolve different types of ribosome pauses. First, for pauses on highly structured RNAs, a slipstream effect likely allows trailing ribosomes to pass regions of RNA structure unhindered after the leading ribosome has unfolded the RNA structure. The magnitude of this slipstream effect is, however, not sufficient to explain the cooperativity of ribosomes translating a structured RNA in our assays (Figure 4H). We speculate that two adjacent ribosomes can also simultaneously pull on the mRNA to produce more force than a single ribosome to unwind the upstream RNA structure, representing a second mechanism of ribosome
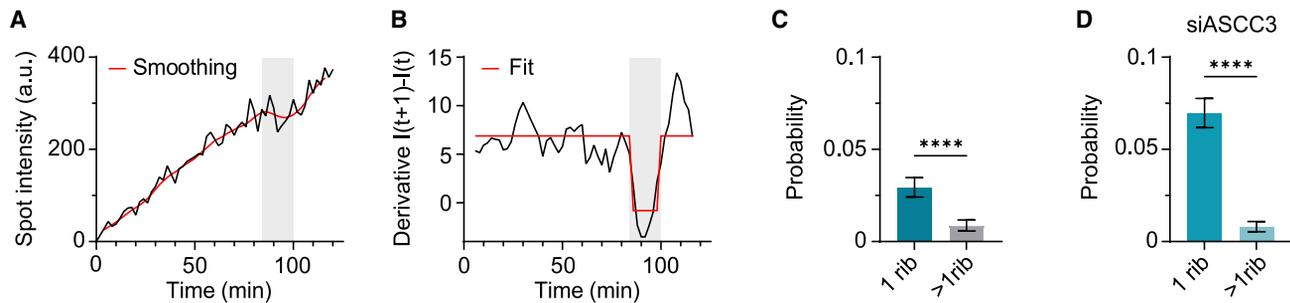
Figure 7. Ribosome cooperativity suppresses stochastic pauses on non-problematic mRNA sequences
(A and B) Example intensity time trace (A) and its derivative (B) show pause identification by Hidden Markov Modeling (B).
(C and D) Probability of pause identification in intensity time traces of untreated socRNAs (C) or socRNAs transfected with ASCC3 siRNAs (D). Number of socRNAs, 1 rib = 170, >1rib = 115 in (C), 1 rib = 328, >1rib = 124 in (D) from 4 experiments. Error bars in (C) and (D) indicate SD, which was calculated using a random sampling method (see STAR Methods). **** indicates $p < 0.0001$ (t test).

cooperativity. Finally, we find that ribosome cooperativity also suppressed pausing in conditions where peptide bond formation was inhibited (e.g., on the Xbp1 pause sequence and pauses induced by anisomycin and narciclasine), suggesting that peptide bond formation may be directly or indirectly stimulated by ribosome collisions. How ribosome collisions could stimulate peptide bond formation is an open question but may involve collision-induced structural rearrangements in the stalled ribosome that alter the peptidyl transferase center, analogous to the activity of the translation factor eIF5A.[35] Intriguingly, ribosome cooperativity also suppresses stochastic pauses during translation of non-problematic sequences (Figure 7), and it will be interesting to determine whether such natural, stochastic pauses are caused by RNA structures or peptide bond formation defects as well.

Ribosome cooperativity suppresses translation surveillance mechanisms
While previous work has established that ribosome collisions can induce ribosome recycling,[36] our data suggest that ribosome collisions can, paradoxically, also suppress recycling of ribosomes. Mechanistically, ribosome cooperativity may inhibit ribosome recycling, at least in part, by reducing pause duration at pause sequences. Since we show that single paused ribosomes are recycled by surveillance mechanisms, pause reduction will likely lead to reduced recycling and thus increased processivity.

A recent study in yeast identified the E3 ubiquitin ligases Mag2 and Fap1, acting in concert with the ribosome quality control trigger (RQT) complex, in sensing and clearing of single, decoding-defective ribosome mutants arrested at the start codon,[33] and in vitro work provided further evidence that single ribosomes can be targeted by surveillance pathways.[37] We show that an analogous quality control pathway exists in human cells that recognizes and removes single ribosomes paused within the CDS. One key difference between our study and the earlier yeast study[33] is that in the earlier work, collisions between scanning 40S ribosomal subunits and the 80S ribosome on the start codon may still occur, while in our experiments there is only a single ribosome per RNA, thus unequivocally demonstrating that single paused ribosomes can be targeted by surveillance mechanisms. Future work will be aimed at determining whether single paused ribosomes on socRNAs are also sensed by Mag2 and Fap1 homologs in humans. Interestingly, we find that single ribosomes are recycled far more efficiently on poly(A) sequences than on Xbp1 or RNA pseudoknot structures, which may reflect pausing in a distinct ribosome conformation on poly(A) sequences, or could be due to recycling factors recruited specifically to poly(A) sequences.[38] SocRNAs represent an invaluable tool to resolve these differences and further dissect quality control pathways targeting single paused ribosomes in the future.

Limitations of the study
To broadly apply socRNAs for studying translation elongation, it is important to consider the limitations of socRNA technology. First, socRNAs lack a 5′ cap, UTRs and a poly(A) tail, so any regulation that requires these RNA elements will not be active on socRNAs. A potential technical concern of socRNAs is that the circular topology of the socRNA may affect translation elongation, for example, by causing mechanical stress. However, we believe mechanical stress is unlikely considering that RNA is an extremely flexible molecule (persistence length ∼1 nm).[39] Moreover, even linear mRNA may form a circular topology under certain conditions.[40] Consistently, we find that translation elongation rates on linear mRNAs and socRNAs are similar. Another potential technical concern is that the very large nascent chains or plasma membrane tethering of socRNAs could affect ribosome translocation. Although we did not find any evidence for this in our experiments (Figures S1O, S2I, and S2J), it is important to include such control experiments in future projects involving socRNAs as well.

CellPress
OPEN ACCESS

Cell
Article

AUTHOR CONTRIBUTIONS

Conceptualization, M.F.M., S.Y., and M.E.T.; data curation, M.F.M. and S.Y.; formal analysis, M.F.M., S.Y., O.W., and M.B.; funding acquisition, S.Y., M.B., and M.E.T.; investigation, M.F.M., S.Y., and M.E.T.; methodology, M.F.M., S.Y., O.W., H.A.S., M.B., and M.E.T.; project administration, M.E.T.; resources, M.F.M., S.Y., O.W., H.A.S., and M.B.; supervision, M.B. and M.E.T.; validation, M.F.M. and S.Y.; visualization, M.F.M., S.Y., O.W., M.B., and M.E.T.; writing, M.F.M., S.Y., and M.E.T. with support from O.W. and M.B.

DECLARATION OF INTERESTS

The authors declare no competing interests.

STAR★METHODS

Detailed methods are provided in the online version of this paper and include the following:

- KEY RESOURCES TABLE
- EXPERIMENTAL MODEL AND STUDY PARTICIPANT DETAILS
  - Cell lines
- METHOD DETAILS
  - Plasmids
  - Cell line generation
  - Microscopy
  - Single-molecule Fluorescence In Situ Hybridization (smFISH)
  - Ribosome processivity under low doses of elongation inhibitors
  - siRNA transfections
  - Sample preparation for socRNA sequencing
  - Simulation
- QUANTIFICATION AND STATISTICAL ANALYSIS
  - Post-acquisition processing of microscopy data
  - Tracking and intensity measurements of socRNA foci
  - Quantification of smFISH results
  - Translation elongation rates of single ribosomes on socRNAs
  - Calculating ribosome pause time
  - Quantification of ribosome processivity
  - Calculating duration of emetine-induced ribosome collisions
  - Calculating off-rates of translation elongation inhibitors
  - Calculating the ribosome cooperativity index
  - Identifying transient pauses in GFP intensity time traces from translated socRNAs
  - Estimation of experimental error using a bootstrapping approach
  - Contribution of cell-to-cell heterogeneity to single ribosome elongation rate heterogeneity
  - Mobility of translating socRNAs
  - Statistical analyses and generation of graphs
- ADDITIONAL RESOURCES
  - Theoretical modeling of ribosome elongation rates heterogeneity

SUPPLEMENTAL INFORMATION

Supplemental information can be found online at https://doi.org/10.1016/j.cell.2025.01.016.

REFERENCES

1. Dever, T.E., Dinman, J.D., and Green, R. (2018). Translation Elongation and Recoding in Eukaryotes. Cold Spring Harb. Perspect. Biol. *10*, a032649. https://doi.org/10.1101/cshperspect.a032649.

2. Collart, M.A., and Weiss, B. (2020). Ribosome pausing, a dangerous necessity for co-translational events. Nucleic Acids Res. *48*, 1043–1055. https://doi.org/10.1093/nar/gkz763.

3. Zhao, T., Chen, Y.M., Li, Y., Wang, J., Chen, S., Gao, N., and Qian, W. (2021). Disome-seq reveals widespread ribosome collisions that promote cotranslational protein folding. Genome Biol. *22*, 16. https://doi.org/10.1186/s13059-020-02256-0.

4. Zhou, Y., Ćorović, M., Hoch-Kraft, P., Meiser, N., Mesitov, M., Körtel, N., Back, H., Naarmann-de Vries, I.S., Katti, K., Obrdlík, A., et al. (2024). m6A sites in the coding region trigger translation-dependent mRNA decay. Mol. Cell *84*, 4576–4593.e12. https://doi.org/10.1016/j.molcel.2024.10.033.

5. Namy, O., Moran, S.J., Stuart, D.I., Gilbert, R.J.C., and Brierley, I. (2006). A mechanical explanation of RNA pseudoknot function in programmed ribosomal frameshifting. Nature *441*, 244–247. https://doi.org/10.1038/nature04735.

6. Hill, C.H., and Brierley, I. (2023). Structural and Functional Insights into Viral Programmed Ribosomal Frameshifting. Annu. Rev. Virol. *10*, 217–242. https://doi.org/10.1146/annurev-virology-111821-120646.

7. Behrmann, E., Loerke, J., Budkevich, T.V., Yamamoto, K., Schmidt, A., Penczek, P.A., Vos, M.R., Bürger, J., Mielke, T., Scheerer, P., and Spahn, C.M. (2015). Structural snapshots of actively translating human ribosomes. Cell *161*, 845–857. https://doi.org/10.1016/j.cell.2015.03.052.

8. Yip, M.C.J., and Shao, S. (2021). Detecting and Rescuing Stalled Ribosomes. Trends Biochem. Sci. *46*, 731–743. https://doi.org/10.1016/j.tibs.2021.03.008.

9. Meydan, S., and Guydosh, N.R. (2021). A cellular handbook for collided ribosomes: surveillance pathways and collision types. Curr. Genet. *67*, 19–26. https://doi.org/10.1007/s00294-020-01111-w.

10. Simms, C.L., Yan, L.L., and Zaher, H.S. (2017). Ribosome Collision Is Critical for Quality Control during No-Go Decay. Mol. Cell *68*, 361–373.e5. https://doi.org/10.1016/j.molcel.2017.08.019.

11. Juszkiewicz, S., Chandrasekaran, V., Lin, Z., Kraatz, S., Ramakrishnan, V., and Hegde, R.S. (2018). ZNF598 Is a Quality Control Sensor of Collided Ribosomes. Mol. Cell *72*, 469–481.e7. https://doi.org/10.1016/j.molcel.2018.08.037.

12. Wu, C.C.C., Peterson, A., Zinshteyn, B., Regot, S., and Green, R. (2020). Ribosome Collisions Trigger General Stress Responses to Regulate Cell Fate. Cell *182*, 404–416.e14. https://doi.org/10.1016/j.cell.2020.06.006.

13. Wang, C., Han, B., Zhou, R., and Zhuang, X. (2016). Real-Time Imaging of Translation on Single mRNA Transcripts in Live Cells. Cell *165*, 990–1001. https://doi.org/10.1016/j.cell.2016.04.040.

14. Yan, X., Hoek, T.A., Vale, R.D., and Tanenbaum, M.E. (2016). Dynamics of Translation of Single mRNA Molecules In Vivo. Cell *165*, 976–989. https://doi.org/10.1016/j.cell.2016.04.034.

15. Morisaki, T., Lyon, K., DeLuca, K.F., DeLuca, J.G., English, B.P., Zhang, Z., Lavis, L.D., Grimm, J.B., Viswanathan, S., Looger, L.L., et al. (2016). Real-time quantification of single RNA translation dynamics in living cells. Science *352*, 1425–1429. https://doi.org/10.1126/science.aaf0899.

16. Pichon, X., Bastide, A., Safieddine, A., Chouaib, R., Samacoits, A., Basyuk, E., Peter, M., Mueller, F., and Bertrand, E. (2016). Visualization of single endogenous polysomes reveals the dynamics of translation in live human cells. J. Cell Biol. *214*, 769–781. https://doi.org/10.1083/jcb.201605024.

17. Wu, B., Eliscovich, C., Yoon, Y.J., and Singer, R.H. (2016). Translation dynamics of single mRNAs in live cells and neurons. Science *352*, 1430–1435. https://doi.org/10.1126/science.aaf1084.

18. Goldman, D.H., Livingston, N.M., Movsik, J., Wu, B., and Green, R. (2021). Live-cell imaging reveals kinetic determinants of quality control triggered by ribosome stalling. Mol. Cell *81*, 1830–1840.e8. https://doi.org/10.1016/j.molcel.2021.01.029.

19. Hoek, T.A., Khuperkar, D., Lindeboom, R.G.H., Sonneveld, S., Verhagen, B.M.P., Boersma, S., Vermeulen, M., and Tanenbaum, M.E. (2019). Single-Molecule Imaging Uncovers Rules Governing Nonsense-Mediated mRNA Decay. Mol. Cell *75*, 324–339.e11. https://doi.org/10.1016/j.molcel.2019.05.008.

20. Litke, J.L., and Jaffrey, S.R. (2019). Highly efficient expression of circular RNA aptamers in cells using autocatalytic transcripts. Nat. Biotechnol. *37*, 667–675. https://doi.org/10.1038/s41587-019-0090-6.

21. Götzke, H., Kilisch, M., Martínez-Carranza, M., Sograte-Idrissi, S., Rajavel, A., Schlichthaerle, T., Engels, N., Jungmann, R., Stenmark, P., Opazo, F., et al. (2019). The ALFA-tag is a highly versatile tool for nanobody-based bioscience applications. Nat. Commun. *10*, 4403. https://doi.org/10.1038/s41467-019-12301-7.

22. Gao, Z., Herrera-Carrillo, E., and Berkhout, B. (2018). RNA Polymerase II Activity of Type 3 Pol III Promoters. Mol. Ther. Nucleic Acids *12*, 135–145. https://doi.org/10.1016/j.omtn.2018.05.001.

23. Gay, D.M., Lund, A.H., and Jansson, M.D. (2022). Translational control through ribosome heterogeneity and functional specialization. Trends Biochem. Sci. *47*, 66–81. https://doi.org/10.1016/j.tibs.2021.07.001.

24. Genuth, N.R., and Barna, M. (2018). The Discovery of Ribosome Heterogeneity and Its Implications for Gene Regulation and Organismal Life. Mol. Cell *71*, 364–374. https://doi.org/10.1016/j.molcel.2018.07.018.

25. Shanmuganathan, V., Schiller, N., Magoulopoulou, A., Cheng, J., Braunger, K., Cymer, F., Berninghausen, O., Beatrix, B., Kohno, K., von Heijne, G., and Beckmann, R. (2019). Structural and mutational analysis of the ribosome-arresting human XBP1u. eLife *8*, e46267. https://doi.org/10.7554/eLife.46267.

26. Yanagitani, K., Kimata, Y., Kadokura, H., and Kohno, K. (2011). Translational pausing ensures membrane targeting and cytoplasmic splicing of XBP1u mRNA. Science *331*, 586–589. https://doi.org/10.1126/science.1197142.

27. Juszkiewicz, S., Speldewinde, S.H., Wan, L., Svejstrup, J.Q., and Hegde, R.S. (2020). The ASC-1 Complex Disassembles Collided Ribosomes. Mol. Cell *79*, 603–e4.e8. https://doi.org/10.1016/j.molcel.2020.06.006.

28. Garzia, A., Jafarnejad, S.M., Meyer, C., Chapat, C., Gogakos, T., Morozov, P., Amiri, M., Shapiro, M., Molina, H., Tuschl, T., and Sonenberg, N. (2017). The E3 ubiquitin ligase and RNA-binding protein ZNF598 orchestrates ribosome quality control of premature polyadenylated mRNAs. Nat. Commun. *8*, 16056. https://doi.org/10.1038/ncomms16056.

29. Lin, J., Zhou, D., Steitz, T.A., Polikanov, Y.S., and Gagnon, M.G. (2018). Ribosome-Targeting Antibiotics: Modes of Action, Mechanisms of Resistance, and Implications for Drug Design. Annu. Rev. Biochem. *87*, 451–478. https://doi.org/10.1146/annurev-biochem-062917-011942.

30. Garreau de Loubresse, N., Prokhorova, I., Holtkamp, W., Rodnina, M.V., Yusupova, G., and Yusupov, M. (2014). Structural basis for the inhibition of the eukaryotic ribosome. Nature *513*, 517–522. https://doi.org/10.1038/nature13737.

31. Arthur, L., Pavlovic-Djuranovic, S., Smith-Koutmou, K., Green, R., Szczesny, P., and Djuranovic, S. (2015). Translational control by lysine-encoding A-rich sequences. Sci. Adv. *1*, e1500154. https://doi.org/10.1126/sciadv.1500154.

32. Niu, X., Sun, R., Chen, Z., Yao, Y., Zuo, X., Chen, C., and Fang, X. (2021). Pseudoknot length modulates the folding, conformational dynamics, and robustness of Xrn1 resistance of flaviviral xrRNAs. Nat. Commun. *12*, 6417. https://doi.org/10.1038/s41467-021-26616-x.

33. Li, S., Ikeuchi, K., Kato, M., Buschauer, R., Sugiyama, T., Adachi, S., Kusano, H., Natsume, T., Berninghausen, O., Matsuo, Y., et al. (2022). Sensing of individual stalled 80S ribosomes by Fap1 for nonfunctional rRNA turnover. Mol. Cell *82*, 3424–3437.e8. https://doi.org/10.1016/j.molcel.2022.08.018.

34. Matsuo, Y., Tesina, P., Nakajima, S., Mizuno, M., Endo, A., Buschauer, R., Cheng, J., Shounai, O., Ikeuchi, K., Saeki, Y., et al. (2020). RQT complex dissociates ribosomes collided on endogenous RQC substrate SDD1. Nat. Struct. Mol. Biol. *27*, 323–332. https://doi.org/10.1038/s41594-020-0393-9.

35. Schuller, A.P., Wu, C.C.C., Dever, T.E., Buskirk, A.R., and Green, R. (2017). eIF5A Functions Globally in Translation Elongation and Termination. Mol. Cell *66*, 194–205.e5. https://doi.org/10.1016/j.molcel.2017.03.003.

36. Kim, K.Q., and Zaher, H.S. (2022). Canary in a coal mine: collided ribosomes as sensors of cellular conditions. Trends Biochem. Sci. *47*, 82–97. https://doi.org/10.1016/j.tibs.2021.09.001.

37. Miścicka, A., Bulakhov, A.G., Kuroha, K., Zinoviev, A., Hellen, C.U.T., and Pestova, T.V. (2024). Ribosomal collision is not a prerequisite for ZNF598-mediated ribosome ubiquitination and disassembly of ribosomal complexes by ASCC. Nucleic Acids Res. *52*, 4627–4643. https://doi.org/10.1093/nar/gkae087.

38. Hildebrandt, A., Brüggemann, M., Rücklé, C., Boerner, S., Heidelberger, J.B., Busch, A., Hänel, H., Voigt, A., Möckel, M.M., Ebersberger, S., et al. (2019). The RNA-binding ubiquitin ligase MKRN1 functions in ribosome-associated quality control of poly(A) translation. Genome Biol. *20*, 216. https://doi.org/10.1186/s13059-019-1814-0.

39. Hyeon, C., Dima, R.I., and Thirumalai, D. (2006). Size, shape, and flexibility of RNA structures. J. Chem. Phys. *125*, 194905. https://doi.org/10.1063/1.2364190.

40. Vicens, Q., Kieft, J.S., and Rissland, O.S. (2018). Revisiting the Closed-Loop Model and the Nature of mRNA 5'-3' Communication. Mol. Cell *72*, 805–812. https://doi.org/10.1016/j.molcel.2018.10.047.

41. Lyubimova, A., Itzkovitz, S., Junker, J.P., Fan, Z.P., Wu, X., and van Oudenaarden, A. (2013). Single-molecule mRNA detection and counting in mammalian tissue. Nat. Protoc. *8*, 1743–1758. https://doi.org/10.1038/nprot.2013.109.

42. Raj, A., van den Bogaard, P., Rifkin, S.A., van Oudenaarden, A., and Tyagi, S. (2008). Imaging individual mRNA molecules using multiple singly labeled probes. Nat. Methods *5*, 877–879. https://doi.org/10.1038/nmeth.1253.

43. Gaspar, I., Wippich, F., and Ephrussi, A. (2018). Terminal Deoxynucleotidyl Transferase Mediated Production of Labeled Probes for Single-molecule FISH or RNA Capture. Bio Protoc. *8*, e2750. https://doi.org/10.21769/BioProtoc.2750.

44. Livingston, N.M., Kwon, J., Valera, O., Saba, J.A., Sinha, N.K., Reddy, P., Nelson, B., Wolfe, C., Ha, T., Green, R., et al. (2023). Bursting translation on single mRNAs in live cells. Mol. Cell *83*, 2276–2289.e11. https://doi.org/10.1016/j.molcel.2023.05.019.

45. Qu, X., Wen, J.D., Lancaster, L., Noller, H.F., Bustamante, C., and Tinoco, I., Jr. (2011). The ribosome uses two active mechanisms to unwind messenger RNA during translation. Nature *475*, 118–121. https://doi.org/10.1038/nature10126.

46. Boersma, S., Khuperkar, D., Verhagen, B.M.P., Sonneveld, S., Grimm, J.B., Lavis, L.D., and Tanenbaum, M.E. (2019). Multi-Color Single-Molecule Imaging Uncovers Extensive Heterogeneity in mRNA Decoding. Cell *178*, 458–472.e19. https://doi.org/10.1016/j.cell.2019.05.001.

47. Bronson, J.E., Fei, J., Hofman, J.M., Gonzalez, R.L., Jr., and Wiggins, C.H. (2009). Learning rates and states from biophysical time series: a Bayesian

approach to model selection and single-molecule FRET data. Biophys. J. *97*, 3196–3205. https://doi.org/10.1016/j.bpj.2009.09.031.

48. Elowitz, M.B., Levine, A.J., Siggia, E.D., and Swain, P.S. (2002). Stochastic gene expression in a single cell. Science *297*, 1183–1186. https://doi.org/10.1126/science.1070919.

49. Swain, P.S., Elowitz, M.B., and Siggia, E.D. (2002). Intrinsic and extrinsic contributions to stochasticity in gene expression. Proc. Natl. Acad. Sci. USA *99*, 12795–12800. https://doi.org/10.1073/pnas.162041399.

50. Rudorf, S. (2019). Efficiency of protein synthesis inhibition depends on tRNA and codon compositions. PLoS Comput. Biol. *15*, e1006979. https://doi.org/10.1371/journal.pcbi.1006979.

51. Rudorf, S., and Lipowsky, R. (2015). Protein Synthesis in E. coli: Dependence of Codon-Specific Elongation on tRNA Concentration and Codon Usage. PLoS One *10*, e0134994. https://doi.org/10.1371/journal.pone.0134994.

Cell
Article

STAR★METHODS

KEY RESOURCES TABLE

REAGENT or RESOURCE	SOURCE	IDENTIFIER
Chemicals, peptides, and recombinant proteins		
DMEM	Gibco	Cat# 31966021
Leibovitz's L15 medium	Gibco	Cat# 21083-027
Penicillin-Streptomycin	Gibco	Cat# 15140-122
Fetal Bovine Serum (FBS)	Sigma-Aldrich	Cat# F7524
Doxycycline	Sigma-Aldrich	Cat# D9891-1G
Opti-MEM	Sigma-Aldrich	Cat# 11058-021
FuGENE 6 Transfection Reagent	Promega	Cat# E231A
Lipofectamine RNAi-MAX	Invitrogen	Cat# 13778-075
TRIsure	Bioline	Cat# Bio-38033
Tetro Reverse Transcriptase	Bioline	Cat# Bio-27036
Polybrene	Santa Cruz Biotechnology, Inc	Cat# sc-134220
Polyethylenimine	Polysciences Inc	Cat# 23966
Puromycin	ThermoFisher Scientific	Cat# 12122530
Harringtonine	Cayman Chemical	Cat# 15361
MG132	Sigma-Aldrich	Cat# M7449
Cycloheximide	Sigma-Aldrich	Cat # C4859
Anisomycin	Sigma-Aldric	Cat # A9789
Emetine	Merck	Cat# 324693
Narciclasine	Cayman Chemical	Cat # 20361
Atto633-NHS	Atto-Tec	Cat# AD 633-31
Amino-11-ddUTP	Lumiprobe	Cat# 15040
Paraformaldehyde	Aurion	Cat# 15710
Formamide	ThermoFischer	Cat# AM9342
Critical commercial assays		
iQ SYBR Green SuperMix	Bio-Rad	Cat# 1708885
GeneJet Gel Extraction Kit	Thermo Scientific	Cat# K0691
Experimental models: Cell lines		
Human U2OS cells	Tanenbaum lab	Cat# HTB-96; RRID:CVCL_0042
HEK293T cells	Tanenbaum lab	Cat# CRL-3216; RRID:CVCL_0063
Recombinant DNA		
See Table S1B for all plasmids used in the paper	This study	N/A
Oligonucleotides		
smFISH probes sequences (5' to 3') gctacctcgttctcaagatg cggaacccttcttcaaacgc agttcttcgagagcagttcc gatcccttttttaatcgagc tgaaagtagttcctcaccac cttcgttttcgaggtggtaa accctgaacctttctttaat tactcagtaattcttcaccc gaaccactcccctttttag ttttcgatagcaattcctcg tttttgagcctagcaacttc	Integrated DNA Technologies (IDT)	N/A

(Continued on next page)

CellPress
OPEN ACCESS

Cell
Article

Continued

REAGENT or RESOURCE	SOURCE	IDENTIFIER
catggtagtattcaccttgc		
cactcggcatggttctacag		
cggccgcactcggcatggtt		
gcttccagatccagatcctg		
ctcagctcttcctccagcct		
ctggctcagtcaggcgtctc		
accggtagaacctccgccac		
ttcttggatagtagctcttc		
cctcgttctcaagatgataa		
acccttcttcaaacgcgcta		
agttcctctcctgagccgga		
gatgatagttcttcgagagc		
tcgagcgacctcattttcaa		
ctgcccgatccctttttaa		
ttgaaagtagttcctcacca		
gtttcgaggtggtaattct		
ttctttaatcgagctacttc		
cttcacccgaccctgaacct		
ataattttttactcagtaatt		
gctacctcattttccagatg		
cactccctttttttagtctc		
tagcaattcctcgccagaac		
tcaagatgataattttttcga		
tgagcctagcaacttcgttc		
gcctgagcctgagccctttt		
gcgcttcttcttgggggtac		
accatggtagtattcacctt		
agtccacgccgaccgcggcc		
cgcactcggcatggttctac		
Deposited data		
Raw data of imaging experiments	This study	Mendeley: 10.17632/yjm7kr86k4.1
Software and algorithms		
ImageJ	NIH	https://imagej.nih.gov/ij/; RRID:SCR_003070
Graphpad Prism 9.4.1	GraphPad Software Inc	http://www.graphpad.com/scientific-software/prism/; RRID:SCR_002798
Matlab R2021b	The Mathworks, Inc.	https://nl.mathworks.com/products/matlab.html; RRID:SCR_001622
Other		
96-well glass bottom imaging plates-(Matriplates)	Brooks Life Science Systems	Cat# MGB096-1-2-LG-L

EXPERIMENTAL MODEL AND STUDY PARTICIPANT DETAILS

Cell lines
Human U2OS cells used for socRNA imaging stably express STAb-GFP or STAb-mStayGold, ALFANb-CAAX, and TetR. All cells were grown in DMEM (4.5 g/L glucose, Gibco) supplemented with 5% fetal bovine serum (Sigma-Aldrich) and 1% penicillin/streptomycin (Gibco) with 5% CO_2 at 37C. Cells were confirmed to be mycoplasma negative.

METHOD DETAILS

Plasmids
The sequences of plasmids used in this study can be found in Table S1A.

Cell line generation
To generate cell lines with stable transgene expression, lentiviral transduction was peformed. Lentivirus was produced in HEK293T cells by transfecting cells at 40 % confluency with a lentiviral plasmid along with the packaging vectors pspax2 and pMD2.g using

Polyethylenimine (PEI) (Polysciences Inc). The cell culture medium was replaced 1 day after transfection, and the supernatant containing lentivirus was harvested 3 days after transfection. For lentiviral transduction, U2OS cells were seeded in 6-well plates and virus-containing supernatant was added to cells together with Polybrene (10 mg/mL) (Santa Cruz Biotechnology Inc). Cells were then spin-infected for 100 minutes at 2000 rpm at 37 ℃. To generate monoclonal cell lines with homogeneous expression levels of the transgenes of interest, single cells were FACS sorted into 96-well plates. A ZNF598 knockout U2OS cell line was generated using CRISPR with the following guide RNA sequence: CTACTGCGCCGTGTGCCGCG.[28]

Microscopy
Microscope
Imaging experiments were performed using a Nikon TI inverted microscope with NIS Element Software equipped with a perfect focus system, a Yokagawa CSU-X1 spinning disc, an iXon Ultra 897 EM-CCD camera (Andor), and a motorized piezo stage (Nanocan SP400, Prior). The microscope was equipped with a temperature-controlled box. A 100x 1.49 NA oil-immersion objective was used for all imaging experiments.

Cell culture for imaging
Unless noted otherwise, socRNA imaging was performed by seeding cells stably expressing STAb-GFP, ALFANb-CAAX, and TetR in a 96-well glass-bottom plate (Matriplates, Brooks Life Science Systems) at ∼25% confluency. The next day, the cells were transfected using Fugene (Promega) with a plasmid encoding the socRNAs of interest. Imaging was done the following day by replacing the medium with pre-warmed imaging medium (CO_2-independent Leibovitz's-15 medium (Gibco) containing 5% fetal bovine serum (Sigma-Aldrich) and 1% penicillin/streptomycin (Gibco)). For socRNAs under the control of a doxycycline-inducible H1 (polIII) promoter, doxycycline (Dox, 1 μg/mL) was added to the cells 90 minutes prior to the start of imaging to induce socRNA expression. For socRNAs under the control of a doxycycline-inducible CMV (polII) promoter, cells were pulsed with doxycycline for 5 minutes, after which doxycycline was removed from the media by subjecting cells to two washing steps using imaging medium. All live-cell imaging experiments were performed at 37°C.

Drug treatment
To precisely determine the number of translating ribosomes on socRNAs, the translation inhibitor puromycin (0.1 mg/mL; ThermoFischer Scientific) was added to cells 1-4 hours after the start of imaging to induce nascent chain release. To prevent potential degradation of nascent polypeptides, the proteasome inhibitor MG132 (10 μM, Merck) was added at the start of imaging for various live-cell imaging experiments (Figures S1L–S1N, 3P, 3Q, 6C, 6D, and S7G). To prevent overloading of the ribosome collision surveillance pathway, harringtonine (3 μg/mL; Cayman Chemical) was added to cells at the start of imaging (Figures 3P and 3Q). To assess the effect of different translation inhibitors on elongation speed, harringtonine (3 μg/mL; Cayman Chemical), or cycloheximide (200 μg/ml) was added to the imaging medium at indicated time-points (Figures 1F and 1G). For studying the binding kinetics of ribosome-targeting drugs (Figures 3K–3O), cycloheximide (25 μg/mL), anisomycin (5 μg/mL), emetine (5 μg/mL), and narciclasine (5 μg/mL) were added to the medium for 15 minutes, followed by subsequent washout through three sequential wash steps with imaging medium.

Single-molecule imaging of socRNAs
For live-cell imaging of socRNAs, the x, y positions for imaging were chosen based on the presence of translated socRNAs in cells. Images were acquired every 90-180 sec for 1-4 hours with exposure times for the 488 nm laser ranging from 50-100 ms. Unless stated otherwise, single z-plane images were acquired with focus on SunTag-GFP foci on the plasma membrane. For experiments in which the GFP fluorescence intensity of individual 24xSunTag arrays was measured, the cells were transfected with a plasmid encoding the 24xSunTag-CAAX protein.

Single-molecule Fluorescence In Situ Hybridization (smFISH)
Probe Labeling for smFISH
smFISH was conducted following established protocols.[41,42] 40 DNA oligonucleotide probes targeting the 5xSunTag socRNA were designed using the Stellaris probe designer tool available at www.biosearchtech.com (key resources table for probe sequences). The labeling of the probes was accomplished using ddUTP-coupled Atto633 dyes (AttoTec) in conjunction with terminal deoxynucleotidyl transferase, as previously detailed.[43] Following probe synthesis, purification entailed precipitation of the labeled probes using 100 % ethanol, subsequent washing with 80% ethanol, and finally resuspension in nuclease-free water.

Probe hybridization
To fix cells for smFISH staining, cells cultured in 96-well glass-bottom plates were first washed once with PBS and then incubated with 4% paraformaldehyde in PBS for 5 minutes at room temperature (RT). Subsequently, cells were subjected to two PBS washes, followed by incubation with 100% ice-cold ethanol at 4 ℃ for 30 minutes. Cells were then washed twice with wash buffer (2xSSC and 10% formamide in diethyl pyrocarbonate-treated water at RT). The labeled smFISH probes were diluted to a concentration of 10 nM in hybridization buffer (1% dextran sulfate, 2xSSC, and 10% formamide in diethyl pyrocarbonate-treated water) and added to the fixed cells, followed by probe hybridization within a sealed container at 37 °C for the duration of 16 hours. To wash away unbound probes, cells underwent two washing cycles with wash buffer lasting 1 hour each at 37 °C. DAPI was included at 1 μg/ml during the

second of the two wash cycles. Finally, cells were washed for another 15 min at RT. For imaging, the wash buffer was replaced with imaging buffer (10 mM Tris pH8, 2xSCC, 0.4% glucose, containing both glucose oxidase (Sigma-Aldrich) and catalase (Sigma-Aldrich)). Imaging was carried out at RT.

Determining the fraction of translated socRNAs for polII and polIII promoters

To determine the fraction of translated cytoplasmic socRNAs originating from polII and polIII promoter constructs (Figure S1I), the same socRNA sequence was first cloned under the control of a doxycycline-inducible H1 and CMV promoter, respectively. U2OS stably expressing STAb-GFP, ALFANb-CAAX and tetR were seeded in glass-bottom 96-well plates and transfected with the respective socRNA plasmids. The next day, cells transfected with the polII socRNA plasmid were pulsed with doxycycline for 5 minutes, after which they were washed twice with imaging buffer to remove doxycycline, incubated at 37 °C for 90 minutes and then fixed with 4% paraformaldehyde. Cells transfected with polIII socRNA constructs were pulsed with doxycycline for 100 minutes, after which they were washed twice with imaging buffer, incubated at 37 °C for 45 minutes and then fixed with 4% paraformaldehyde. Note that different doxycycline treatment regimes were used because the transcription induction dynamics in response to doxycycline treatment of the two promoters is different. After fixation, smFISH staining was performed as described above. Cells were imaged at RT. To capture the whole 3D volume of the cells, z-slices were acquired at 400nm intervals.

Dual-color experiments to interrogate the mechanism of translation initiation on socRNAs

SocRNA reporters designed to interrogate the mechanism of translation initiation (Figures S1L–S1N) were transfected into U2OS cells stably expressing STAb-GFP, ANFANb-Halo and tetR. The next day, socRNA expression was induced by addition of doxycycline. To ensure that socRNA translation products were not degraded, the proteasome inhibitor MG132 (10 μM, Merck) was added to cells. 2.5 hours after doxycycline addition, cells were washed twice and incubated with 50 nM Halo-JFX650 for 30 minutes, after which cells were washed twice to remove unbound dye. Three hours after the initial addition of doxycycline, cells were treated with puromycin for 15 minutes and then fixed with 4% paraformaldehyde for 5 minutes. Imaging of fixed cells was done in PBS at RT with z-stacks with 300 nm intervals between images. Maximum intensity projections were generated and the Fiji plugin Comdet was used to quantify the number of GFP and JFX650 foci per cell. Foci positive for both GFP and JFX650 signal, which likely represent ribosome frameshifting products, were excluded from the analysis.

Comparison of tethered versus untethered socRNA translation

To compare the translation speed of ribosomes that are untethered versus tethered to the plasma membrane through their nascent chain (Figure S1O), polII socRNA plasmids were transfected into cells expressing STAb-mSTayGold, tetR and either expressing or lacking the ALFANb-CAAX used for tethering socRNA translation sites to the plasma membrane. After transfection, cells were pulsed with doxycycline for 5 minutes to induce socRNA expression during a short time window, and puromycin was added to cells after 60, 90, 120 and 180 minutes to release all ribosome nascent chains. 20 minutes after puromycin addition, cells were fixed using 4% paraformaldehyde for 10 minutes. Cells were imaged at RT in PBS with z-slices taken at 400nm intervals to capture the whole 3D volume of cells. The Fiji plugin Comdet was used to measure the median intensity of ∼500 socRNA translation products from maximum intensity projections for each condition. For the socRNA used in these experiments, 68% were translated by single ribosomes and 32% by two or more ribosomes. Since the distribution of GFP intensities is indistinguishable for tethered and untethered socRNAs (Figure S1O), these results show that both single and multiple ribosomes on a socRNA translated at a similar rate when socRNAs are tethered to the plasma membrane.

Ribosome processivity under low doses of elongation inhibitors

To determine the effect of low doses of elongation inhibitors on socRNAs translated by either one or two ribosomes (Figures S5B–S5E), socRNA expression was induced and cells were selected for imaging. Upon start of imaging, harringtonine was added to cells (3 μg/mL, Cayman Chemical) to induce run-off of all translating ribosomes to prevent the occurrence of widespread ribosome collisions on endogenous mRNAs and potential overloading of collision sensing pathways. 30 minutes after Harringtonine addition, low doses of elongation inhibitors (emetine at 0.1 μg/mL, anisomycin at 0.03 μg/mL, and narciclasine at 0.03 μg/mL) was added to cells. Together with the respective elongation inhibitor, MG132 (10 μM) was added to cells to prevent potential degradation of socRNA translation products as a consequence of RQC. socRNA translation sites were imaged and tracked for another 100 minutes, after which puromycin was added to cells to determine the number of translating ribosomes per socRNA. In the case of nascent chain release or ribosome recycling, which results in splitting of the socRNA translation site initially translated by two ribosomes, the intensities of both daughter spots were still followed and measured for inclusion in the analysis.

siRNA transfections

Cells were first reverse transfected with siRNAs at a final concentration of 10 nM using Lipofectamine RNAiMAX (Invitrogen) and seeded in 96-well glass-bottom imaging plates. After 24hr, the cells were trypsinized, transfected with a second dose of 10 nM siRNA, and re-plated in 96-well glass-bottom imaging plates. 24 hr after the second siRNA transfection, cells were transfected with plasmid DNA encoding a socRNA, as described above. 24 hr after DNA transfection, imaging coxperiments or/and qPCR were performed. The sequences of the siRNAs used in this study are listed below.

Cell
Article

ZNF598: 5'-ACGAGGAGGUGGACAGGUAUU-3' (Dharmacon)
ASCC3: 5'-GAUAAAGCGAUCUAAACUUUU-3' (Dharmacon)
Kif18b (used as a Control siRNA): TTGATGACTGTGGCTGGGC (Dharmacon)

siRNA knockdown efficiency

To determine the knock-down efficiency of siRNAs, RNA from siRNA-treated cells was isolated using TRIsure (Bioline). Next, cDNA was synthesized using Random hexamers and Tetro Reverse Transcriptase (Bioline). Quantitative PCRs (qPCRs) were performed using SYBR-Green Supermix (Bio-Rad) on a Bio-Rad Real-time PCR machine (CFX Connect Real-Time PCR Detection System). mRNA levels were determined by qPCR. If the quantitation cycle (C_q) of a sample was higher than that of a water control, the sample was excluded from analysis. GAPDH and Ribophorin were used as reference genes and fold changes were calculated using the ΔΔCt method. The sequences of the oligonucleotides used for qPCR are listed below (5' – 3').

ZNF598	(FWD) GGAACGAGGGGGTCGTTG	(REV) TTGTACCTCCAGCTTCCTCG
ASCC3	(FWD) ATCAAATTGCATGCTGACCA	(REV) TGATTTGGGAAATCGAGGAG
GAPDH	(FWD) CACCGTCAAGGCTGAGAACGGG	(REV) GGTGAAGACGCCAGTGGACTCC
Ribophorin	(FWD) GAGGGCTCTGATCTGTGCGACAG	(REV) GCCAGCCACCAGGCGCTCAG

Sample preparation for socRNA sequencing

To validate the sequence of socRNAs (Figure S2G), RNA was isolated from cells 3 hours after inducing socRNA expression using TRIsure (Bioline). Subsequently, cDNA was synthesized utilizing a gene-specific primer designed to target the 10xSunTag socRNA and Tetro Reverse Transcriptase (Bioline). The resulting cDNA was isolated via column-based purification using the GeneJet Gel Extraction Kit (Thermo Scientific). To generate dsDNA for sequencing using the cDNA as template, three distinct polymerase chain reaction (PCR) reactions were performed to amplify regions which together cover the entire socRNA sequence. Following purification of the PCR products, each PCR product was sent for Sanger sequencing together with the reverse primer used in the corresponding PCR.

Simulation
Modelling ribosome translocation dynamics in silico

To investigate the prevalence of ribosome collisions on mRNAs, we simulated translation of ribosomes over time using a computational model. In the model, ribosomes moved one codon at a time with a variable rate representing the stochastic behavior of ribosome translocation. The time it takes a ribosome to move one codon was determined by randomly selecting a value from a distribution that represented the elongation cycle duration. This elongation cycle duration distribution was constructed in the following way:

(1) We determined that the average of the elongation cycle distribution is 3 aa/s, in accordance with previously calculated elongation speed values on linear mRNAs in our cell line.[14]

(2) Based on a previously published CryoEM dataset of ribosome elongation,[7] the entire elongation cycle was first divided into 7 distinct sub-steps that ribosomes cycle through.

(3) The relative abundance of each individual sub-step structure (0.0833, 0.0315, 0.0833, 0.25, 0.396, 0.0833 and 0.073 determined in Behrmann et al.[7]) was used to first calculate the average duration of each sub-step. Specifically, average sub-step durations were calculated by multiplying the relative abundance of each sub-step by the duration of the entire elongation cycle. Next, for each sub-step, a duration distribution was constructed following a single exponential decay function with a mean determined as described above (See Figure 2E). The sum of the averages from all 7 sub-step distributions is exactly 3 aa/s, equal to the ribosome elongation speed as previously determined on linear mRNAs.[14] It is important to note that relative occurrence of structures in EM images provide only rough estimates of the duration of sub-steps, and precise in vivo values may differ.

(4) To construct the distribution of durations for one entire elongation cycle, a duration for each individual sub-step was randomly selected from the distributions constructed in (3) and these seven durations were summed. This process was repeated 5 million times to construct the distribution of durations of one elongation cycle (See Figure 2F).

(5) For each translated codon, we randomly picked a value from the distribution described in (4) to determine how long it takes to translate that codon.

(6) To simulate the experimentally observed heterogeneity in elongation rates for individual ribosomes (Figures 2A–2D), each individual ribosome was assigned a relative elongation speed picked at random from a Gaussian distribution which was based on the actual elongation speed heterogeneity (mean of 1, coefficient of variation = 0.158). For every individual ribosome, each new elongation cycle duration was divided by the relative elongation speed of that ribosome.

In all simulations, the ribosome footprint size was set to exactly 10 codons, and ribosomes colliding with a slower leading ribosome could not overtake the leading ribosome.

For simulations in which the elongation cycle consisted of 1 rate-limiting sub-step (See Figures S3C–S3E, S3H, and S3I) we exchanged the values described in (2) such that one sub-step took up two thirds of the entire elongation cycle duration. Specifically, the 7 values were changed to 0.667, 0.056, 0.056, 0.056, 0.056, 0.056 and 0.056.

Simulating ribosome collisions on endogenous linear mRNAs

Translation initiation was simulated using an average interval of 30 seconds between initiation events, in accordance with experimentally determined ribosome initiation rates.[14,44] To stimulate the stochasticity of translation initiation kinetics, the interval between two initiation events was picked randomly from a distribution that followed a single exponential decay with a mean of 30 s. Since a ribosome cannot initiate translation until the previous ribosome is at least 10 codons downstream of the initiation site, we introduced a minimum interval between initiation events of 10 s, reflecting the combined time of translation initiation and translation of 10 codons (Figure S3F). In parallel, additional simulations were performed in which the interval between initiation events was shorter and translation elongation rates were somewhat higher (~13s and 4.8 codons/s, respectively, in line with measurements of another study.[44] Finally, simulations were performed in which the interval between two initiation events on an mRNA was picked from a Gaussian rather than an exponential decay distribution (mean = 30, sd = 15, with values smaller than 3 s removed from the distribution) (Figure S3G). After initiation, ribosome translocation was simulated for 30 min, as described above. For each simulated mRNA, the fraction of all ribosomes which at some point collided with another ribosome was calculated.

Simulating ribosome collisions on socRNAs

To model the time and number of codons translated (per ribosomes) until the first collision between 2 ribosomes translating the same socRNA, ribosomes were initially loaded at random but nonoverlapping locations on the socRNA. To match our experimental data, the socRNA used in this simulation had a length of 175 codons and ribosomes translated with an average speed of 2.6 aa/s, consistent with our experimental measurements. In addition, intrinsic ribosome heterogeneity in speed was incorporated in this simulation, as described above. Translation elongation was initiated *in silico* and the time and number of codons translated until the first collision occurred were recorded for 1000 simulations.

Ribosome interference during translation on socRNAs without pause sequence

To quantitatively assess how translating ribosomes influence each other's translocation dynamics on socRNAs, we conducted simulations in which two ribosomes translate the same socRNA simultaneously.

We used the following parameters for these simulations:

(1) We used the same socRNA lengths as those used in the experiments (in number of codons).
(2) We randomly selected a value for the intrinsic, average ribosome speed for each ribosome, based on the intrinsic ribosome speed distribution. This distribution was obtained from the same cell line (mean = average ribosome elongation speed (aa/s) acquired from experimental data, coefficient of variation = 0.16).
(3) We determined the translation initiation time for each ribosome as described in modelling ribosome translocation dynamics in silico.
(4) A ribosome can only move forward by one codon if the second ribosome is >10 codons away (based on a ribosome footprint of 30 nt = 10 codons).

Using the parameter described above, combined with the translation elongation dynamics simulations described in modelling ribosome translocation dynamics in silico, we conducted simulations of ribosome translocation and measured ribosome translocation rates.

We converted total amino acids translated by each ribosome into a GFP intensity time trace to mimic experimental data (Figures 4A and 4B). To do this, we used the single GFP molecule intensity as described in translation elongation rates of single ribosomes on socRNAs. For example, for the socRNA template encoding 10xSunTag, the total number of codons for one cycle is 321 codons and the total number of GFPs synthesized in one cycle is 10. We thus divided 10x(single GFP intensity) by 321 to determine the average GFP increase per codon.

Ribosome interference during translation on socRNAs with pause sequence

In the simulations where two ribosomes translate the same socRNA encoding a pause sequence, we used the same computational framework described above, but implemented the following the changes:

(1) A pause site was inserted into the socRNA.
(2) A ribosome undergoes a pause when it translates the last codon of the pause site.
(3) The pause time for each pausing event is determined by randomly drawing a value from an exponential decay distribution with a mean value that is based on experimental measurements for socRNAs containing that pause sequence. For mean pause durations the pause time for single ribosomes translating the socRNA was used.

Slipstream effect with RNA structures

In simulations where two ribosomes translate the same socRNA encoding a pseudoknot RNA structure, we introduced the following adjustments to account for the 'slipstream' effect associated with translation of an RNA structure by multiple ribosomes:

(1) A pseudoknot, spanning a length of 26 codons, was inserted into the socRNA.

(2) To simulate ribosome pausing upstream of the pseudoknot, we incorporated the requirement in our simulations that when a ribosome has codon 'i' in the A site, translocation to the next codon requires the unwinding of codon 'i+4' downstream.[45] This results in a ribosome pause occurring 4 codons upstream of the first codon of the pseudoknot.

(3) The duration of ribosome pausing upstream of the pseudoknot is equal to the unfolding time of the pseudoknot structure, which was determined in our simulations by randomly drawing a value from an exponential decay distribution with a mean value equal to the average pause time of single ribosomes on socRNAs encoding the pseudoknot.

(4) After unfolding of the pseudoknot structure, the ribosome resumes translation and translates the pseudoknot sequence at the same speed as non-pseudoknot sequences are translated at.

(5) Slipstream effect: if a ribosome translates the codon that is 4 codons upstream of the first codon of the pseudoknot (referred to as 'i'), and the other ribosome (which has a 30 nt footprint) is still covering part of the pseudoknot sequence with its footprint, the trailing ribosome does not pause at codon 'i-4'. This is because the leading ribosome has already unfolded the pseudoknot structure and prevents its refolding when the ribosome footprint covers the pseudoknot sequence.

Ribosome cooperativity on socRNAs with a pause sequence

To incorporate ribosome cooperativity in the simulation where two ribosomes translate the same socRNA encoding a pause sequence, the same parameters were used as described in ribosome interference during translation on socRNAs with pause sequence, but with the following modifications:

When a leading ribosome pauses at the pause site (codon 'i') and a trailing ribosome has codon 'i-5', in the A site, i.e., a translating ribosome collides with the paused ribosome, the paused ribosome automatically translocates to the next codon, irrespective of the pause duration that was drawn from the pause time distribution. In the simulations in Figures S6A and S6B, we also included a delay time between collision and automatic translocation of the paused ribosome. We used different delays after collision (e.g., 0, 10, 20, 40 seconds for Xbp1(S255A)). In the simulations in Figures S6C and S6D, we included different probabilities of cooperativity for which collision-induced resumption of translation happens with certain probability. For example, 0 % indicates no cooperativity as same as ribosome interference simulation.

Simulating ribosome run-off experiments

To simulate experiments for which ribosome run-off was induced by harringtonine treatment on a linear mRNA encoding an Xbp1(S255A) pause site (Figure 4K), ribosomes were randomly deposited on the mRNA in silico. For each simulated mRNA, the number of deposited ribosomes was randomly drawn number from a distribution representing the experimentally determined distribution of ribosome number per mRNA (Figure S5H). Run-off experiments were simulated according to the 'ribosome interference' model (Figure 4B). Simulations ran until all ribosomes had run off the mRNA. In parallel, simulations were also performed in accordance with the 'ribosome cooperativity' model (Figure S6A), which assumed that collisions lasted for 40 s before the leading ribosome resumed translation. This time delay of 40 s best fit the experimental data for ribosome cooperativity on socRNAs encoding the Xbp1(S255A) pause site (Figure S6A). The position of each ribosome along the mRNA was recorded at each time-point during the simulation. Using the ribosome position information, the number of SunTag epitopes associated with each ribosome, which directly corresponds to the GFP intensity of each translated SunTag mRNA, was calculated over time. Ribosomes located at or downstream of codon 640 (reflecting the combined length of the 24xSunTag array and the ribosome exit tunnel length of 40 amino acids) had synthesized 24x fully exposed SunTag epitopes in the simulations. Ribosomes present at codons upstream of codon 640 had only synthesized and exposed a fraction of the N-terminal 24xSunTag array. For ribosomes upstream of codon 640, the fraction of exposed SunTag peptides was calculated by dividing the codon position by 640. Finally, to determine the average GFP intensity associated with all ribosomes in the simulations of ribosome run-off, for each time point, the average spot intensity from all simulated mRNAs containing at least one ribosome was calculated and multiplied by the total number of mRNAs still containing at least one ribosome.

QUANTIFICATION AND STATISTICAL ANALYSIS

Post-acquisition processing of microscopy data

For all images, flat-field correction was performed using images obtained from concentrated dye solutions (4 μg/mL DyLight™ 488 NHS Ester for 488 laser line, and 40 μg/mL Alexa Fluor™ 555 NHS Ester for 561 laser line) and dark current images.

For experiments investigating single ribosome heterogeneity in translation elongation rates (Figures 2A–2D), we wanted to correct for possible drift in the z-direction, since foci intensity changes slightly even when foci move <100 nm in z. Therefore, 9 z-slices were acquired with a 2 μm total z distance surrounding the GFP foci. Foci intensity was measured in each z slice to acquire a Gaussian profile of GFP foci in the z-direction. To capture the maximum intensity of individual GFP foci at each time point, we first summed the intensity values of 3 adjacent slices across the different z-positions at each pixel, resulting in total 7 summed intensity values at each pixel (This approach is conceptually similar to a moving average over a sliding window length of 3). Then, we used the maximum value among the 7 summed-values for each pixel to generate a maximum intensity projection image at each time point. The reason we used the maximum value of the summed values of 3 adjacent slices instead of a maximum intensity projection is to avoid maximizing the background intensity from the non-GFP foci area.

Tracking and intensity measurements of socRNA foci

For tracking and fluorescence intensity measurements of socRNAs, we used the 'TransTrack' software package as previously described.[46] To encompass the entire GFP foci, we applied an ROI size that was sufficiently large to capture the entire GFP spot in all cases (8x8 pixels) for the intensity quantification. All resulting traces underwent manual curation to ensure accuracy.

To correct for photobleaching of membrane-tethered GFP-foci, we used GFP intensity time traces from foci exhibiting no increase in intensity over time, referred to as 'non-translating traces' (Figure S2P), which were acquired in the same imaging experiments. We confirmed these were indeed 'non-translating traces' by comparing the traces acquired under puromycin condition (Figure S2R). The decrease in fluorescence intensity of these non-translating GFP foci over time was fit with a single exponential decay function to determine the bleaching rate. All GFP foci intensities were then corrected for the photobleaching (Figure S2Q). We used the photobleaching corrected non-translation traces as 'plateau traces' for further analysis. We found that bleach correction on GFP foci rather than whole cell fluorescence is essential, as GFP foci bleach faster than the whole cell, because only a small region of the cell in the z-direction is excited by laser light, while GFP foci stay within the excitation focus plane throughout the experiment and thus bleach faster than the whole cell fluorescence.

In a small number of cases, GFP foci rapidly disappeared during imaging, which may reflect protein decay. Such rapid GFP foci disappearance almost always occurred after translation termination and therefore does not interfere with our measurements on translation elongation

Experimental details including number of repeats, cells, and spots per experiment are described in Figure legends and in Table S1B.

Quantification of smFISH results

To assess the co-localization of smFISH spots with socRNA translation sites (Figure S1B), socRNA translation sites were first imaged and tracked over time, followed by smFISH staining of the same cells. Combining live-cell imaging and smFISH of the same cells allowed us to determine co-localization of smFISH RNA foci for both translated and non-translated socRNAs. After live-cell imaging, cells were quickly fixed, smFISH staining was performed and the same cells were imaged again to co-localize smFISH signal and socRNA translation signal, which was preserved after fixation. Intensity threshold-based masks were generated for each SunTag-positive object, and the presence or absence of a co-localizing smFISH spots was scored using the Fiji plugin Comdet. To control for chance co-localization, the far-red channel (smFISH signal) was rotated by 90 degrees relative to the green channel (socRNA translation products), and the same analysis was carried out again.

For determining the fraction of translated socRNAs originating from polII versus polIII promoters (Figure S1I), the total number of smFISH spots per cell was first measured from maximum intensity projections using the Fiji plugin ComDet. A DAPI-positive mask was used to measure the number of nuclear smFISH spots in each cell, which was subtracted from the total number of smFISH spots to calculate the number of cytoplasmic socRNAs in each cell. Next, to determine the absolute number of translated socRNAs per cell, intensity threshold-based masks were made for each cell that contained SunTag GFP foci and the presence or absence of a co-localizing smFISH spots was scored for each GFP spot using the Fiji plugin Comdet. To control for chance co-localization, the far-red channel (smFISH signal) was rotated by 90 degrees relative to the green channel (socRNA translation products), and the same analysis was carried out again. Finally, to calculate the fraction of cytoplasmic socRNAs that are translated, the total number of translated socRNAs in each cell was divided by the total number of cytoplasmic socRNAs measured in each cell.

Translation elongation rates of single ribosomes on socRNAs

To determine the number of translating ribosomes per socRNA, puromycin (0.1 mg/mL) was added to cells at the end of the imaging experiment and the number of ribosomes was determined by counting the number of splitting GFP foci after puromycin addition (Figures 1J and 1K). If GFP foci split off from the translated socRNA before puromycin addition (Figure S1G), these events were incorporated into the analysis. The elongation rate of ribosomes on socRNAs was determined by fitting a linear function to GFP intensity time traces to extract the slope of intensity increase phase before puromycin addition. Also, when GFP foci split into multiple foci over the course of the experiment, we took the intensity traces until the moment of foci splitting to extract the slope of intensity increase phase before foci splitting. The slope was then divided by the number of ribosomes to determine the translation elongation speed per ribosome. To convert rates of GFP intensity increase into the unit of amino acids translated per second, we first determined the intensity of a single GFP molecule under our experimental settings. To achieve this, we measured the intensity of individual 'mature' SunTag proteins containing 24 repeats of the SunTag peptide fused to a CAAX motif (24xSunTag-CAAX) using the same settings as those used in the imaging experiment. We divided the average intensity of 24xSunTag-CAAX foci by 24 to obtain the intensity of a single GFP molecule. Using the intensity of a single GFP molecule, we could calculate the number of SunTag epitopes synthesized per unit of time for translated socRNAs. Next, for each socRNA, we calculated the average number of codons that need to be translated for the synthesis of one SunTag epitope; we determined the number of codons for the translation of a full cycle for each socRNA, and the number of SunTag epitopes synthesized upon translation of the socRNA once (equal to the number of SunTags encoded in a socRNA, 5 or 10, unless noted otherwise). Based on the number of codons in one full cycle of socRNA translation and the number of SunTags encoded in a socRNAs, we calculated the elongation rate in amino acids per second.

To investigate single ribosome heterogeneity in translation elongation rates (Figures 2A–2D), technical noise in intensity time traces was evaluated using control intensity time traces (Figure 2B). Specifically, the intensities of GFP foci that displayed no increase in

Cell
Article

CellPress
OPEN ACCESS

intensity ('plateau traces') were measured over time. These intensity measurements were transformed using the mean slope of the intensity time traces corresponding to single ribosomes translating socRNAs (black dotted line in Figure 2A). Only socRNAs translated by a single ribosome were included in the analysis.

Calculating ribosome pause time

To determine ribosome pause time on socRNAs encoding a pause sequence, we determined the average elongation rates (i.e., the total time to complete translation of one full circle, which represents the time needed to translate the non-pause sequence plus the pause time on the pause sequence) of single ribosomes as described in the paragraph above. We then subtracted the average translation time for one cycle of translation of a matched socRNA lacking the pause sequence to obtain the pause duration per cycle.

Quantification of ribosome processivity

To determine the number of codons translated by individual ribosomes on socRNAs, we tracked GFP intensity time traces for translated socRNAs and determined the moment when the GFP intensity stopped increasing for individual translated socRNAs. For socRNAs translated until puromycin addition, we noted the last frame before puromycin addition as the last time-point in which translation was detected. We then measured for each individual socRNA the GFP foci intensity at the last time-point of translation and calculated the total number of codons translated during the experiment based on this final time-point GFP intensity, as described in translation elongation rates of single ribosomes on socRNAs. The fraction of translated socRNAs remaining was then plotted against the total number of codons translated in Kaplan-Meier survival plots.

For socRNAs that were translated by two ribosomes, we determined the moment when the GFP foci split into two foci and kept tracked the intensity of both foci to determine whether one of foci intensities continued increasing (indicating that one of the two ribosomes continued translating) or whether both foci stop increasing in intensity (indicating that both ribosomes aborted translation) after splitting. We then measured the GFP foci intensity at the moment of foci splitting and calculated the total number of codons translated based on the GFP intensity. Next, the total number of translated codons was divided by two to determine the number of codons translated by each ribosome. To compare processivity of single or multiple ribosomes translating a socRNA, the fraction of translating ribosome was plotted against the total number of translated codons per ribosome between as Kaplan-Meier survival curves. For socRNAs translated by two ribosomes, we determine the moment of splitting (indicative of the first ribosome aborting translation), and noted that moment as aborted translation for one ribosome and as the last moment that translation could be detected for the other ribosomes.

Calculating duration of emetine-induced ribosome collisions

We wanted to quantitatively assess the moment from ribosome collision until ribosome recycling in emetine-induced ribosome collisions (Figures 3P and 3Q). We first titrated emetine concentration to very low levels (Figure S4F) to ensure that only one ribosome per socRNA was targeted by the elongation inhibitor, so that the other ribosome(s) could collide with the emetine-arrested ribosome. To prevent overloading of the cell-wide ribosome collision surveillance pathway upon low-dose emetine addition, potentially titrating away recycling factors, harringtonine was added to cells 30 minutes prior to emetine addition, which results in ribosome run-off on endogenous linear mRNAs, but not on socRNAs. GFP foci were tracked before and after emetine addition and the foci intensities were plotted over time. Upon binding of emetine to one of the two ribosomes, a transition from a positive slope to a plateau is observed in the GFP intensity time trace, where the transition point represents the moment of emetine-induced ribosome pausing. To identify this transition time point, we fit the GFP intensity time traces with two distinct linear regression models such that the two-state regression model best fit the data using the least squares approach (Figure S4G). Importantly, the second of the two linear regression model was constrained to have a slope of zero to fit the paused state, and the first linear regression model needed to exhibit a positive slope to fit the trace up until the moment of ribosome pausing. The intersection point between the two regression models was used to calculate the moment in time of collision onset, and the time interval between collision onset and visible splitting of socRNA translation spot into two daughter spots was calculated. To precisely determine the collision duration from the moment of collision onset to the moment of ribosome recycling, we corrected for the time needed from the moment of ribosome recycling until the two GFP foci have diffused sufficiently far apart from each other to be scored as a ribosome splitting. To determine this time, socRNAs translated by two ribosomes were imaged and treated with puromycin and the time from puro addition until splitting was recorded (Figure S4H, single exponential function: half-life = 1.4 min, tau = 2.0). In addition, we also corrected for the average duration needed for two ribosomes to collide upon emetine binding to one of the two ribosomes. For this calculation we assumed that the relative distance between the two ribosomes on the socRNA is half the length of the socRNA (i.e., that they are randomly positioned relative to each other) (average time = 0.5 min on socRNA with a size of 525 nt and elongation speed of 2.6 aa/s). Both the average time needed for GFP foci diffusion and for collision upon emetine binding were subtracted from our data to calculate the duration of ribosome collision until the moment of recycling.

Calculating off-rates of translation elongation inhibitors

To quantitatively assess binding kinetics of elongation inhibitors, we generated intensity time traces of translated socRNAs from cells treated with elongation inhibitors, followed by inhibitor washout. To identify the moment of dissociation of the translation inhibitor, we wished to identify the precise moment in time when the GFP intensity time trace transitions from a plateau to a positive slope. To

identify this transition point, a custom-written python script was applied, which employed two distinct linear regression models to fit the intensity time trace. The least squares method was used to find an optimal fit. The linear regression model for the first half of the intensity time trace was constrained to have a slope of zero (representing the time when the inhibitor is still bound to the ribosome), while the linear regression model for the second part of the intensity time trace needed to exhibit a positive slope (representing the time when the inhibitor was released from the ribosome and translation had resumed).

Calculating the ribosome cooperativity index

The cooperativity index represents a measure for the degree to which the presence of a second ribosome speeds up the translation elongation speed of another ribosome. The cooperativity index was calculated for socRNAs containing a pause site. To calculate the cooperativity index, we first calculated the average total pause time per full cycle of socRNA translation per ribosome. The total pause time includes both the pause on the pause site (e.g., Xbp1 sequence) and the 'waiting time' in which a trailing ribosome is paused upstream of a ribosome that is paused on the pause site (which is referred to as ribosome interference). The total pause time is calculated from the ribosome interference simulation as described in ribosome interference during translation on socRNAs with pause sequence (e.g., black data in Figures 5A and 5B). To calculate the cooperativity index, the calculated total pause time per ribosome was divided by the pause time per ribosome determined from the experiments (e.g., cyan data in Figures 5A and 5B). The cooperativity index indicates how much the total pause time is reduced by second ribosome.

Identifying transient pauses in GFP intensity time traces from translated socRNAs

To identify pauses within the intensity time traces (Figures 7A and 7B), the intensity value of each time point in the raw intensity traces (black line in Figure 7A) was first divided by the number of ribosomes on that socRNA to calculate the elongation rate per ribosome. Next, the intensity traces were smoothed using a 6-point moving median to eliminate outlier data points. Subsequently, a 5-point moving average was applied to further smooth the data (red line in Figure 7A). Following smoothing, the first derivative, which represents the differences between adjacent intensities, was calculated (black line in Figure 7B). Pause identification was performed using a Hidden Markov Model (vbFRET algorithm[47] with default settings of the algorithm. To compare pause frequency between one ribosome traces and multiple ribosomes traces, identical threshold for defining pause state were used for both data set.

Estimation of experimental error using a bootstrapping approach

The estimation of the experimental error, as indicated by the error bars in Figures 7C and 7D, was performed using a bootstrapping approach, because the sample size per experiment was too small for reliable use of the standard deviation. Specifically, 1000 *in silico* samples were generated by randomly selecting data values from the original dataset, utilizing the *randi* function in Matlab. After drawing each data point, the data point was returned to the original data set from which data points are drawn. The error bars represent the standard deviation for these 1000 simulated samples. The original dataset for each condition was compiled from 4 independent experiments.

Contribution of cell-to-cell heterogeneity to single ribosome elongation rate heterogeneity

To quantify the contribution of cell-to-cell heterogeneity to single ribosome elongation rate heterogeneity, we randomly selected two ribosomes translating two different socRNAs within the same cell (Figure S2F) and employed an approach used for the noise decomposition into intrinsic and extrinsic components, which have orthogonal contribution to total noise (Figure S2G).[48,49] In brief, the total noise (defined as the standard deviation divided by the mean) in the ribosome elongation rates (Figure 2C) can be separated into two components: intrinsic noise (e.g., variation between ribosomes) and extrinsic noise (e.g., variation between cells). Extrinsic noise corresponds to the data spread parallel to the diagonal line on the scatter plot showing the speed of the two randomly selected ribosomes from the same cell (Figure S2F). On the other hand, intrinsic noise is represented by the data spread perpendicular to the diagonal line on the scatter plot. Intrinsic, extrinsic, and total noise were defined as follows:

$$\eta^2_{intrinsic} = \frac{\langle (V1 - V2)^2 \rangle}{2 <V1><V2>}; \ \eta^2_{extrinsic} = \frac{<V1V2> - <V1><V2>}{<V1><V1>}; \ \eta^2_{total} = \eta^2_{extrinsic} + \eta^2_{intrinsic}$$

where $V1$ and $V2$ represent the elongation rates of either of two ribosomes randomly picked from the same cell, respectively. Angled brackets denote means over the cell population. Based on this approach, we calculated that only $\sim$22% of the ribosome speed variation originates from extrinsic noise, i.e., cell-to-cell heterogeneity, with the majority of variation originating from intrinsic noise.

Mobility of translating socRNAs

To acquire the x, y coordinates of individual translating socRNAs at each time, we tracked the socRNAs using TransTrack[46] with 90 s time intervals. Using the x, y position information of foci at each time point, we calculated the mean squared displacement as a measure of the mobility of translating socRNAs.

Cell
Article

Statistical analyses and generation of graphs

All graphs were generated using Prism GraphPad (v9) or in python 3.10 using Matplotlib. Details of statistical tests for each graph are explained in figure legends.

ADDITIONAL RESOURCES

Theoretical modeling of ribosome elongation rates heterogeneity
Main results

We consider the single ribosome translation traces, and investigate the heterogeneity observed in the estimated translation elongation rates $\widehat{k}$. In particular, we ask the question if the heterogeneity in $\widehat{k}$ can be explained by a combination of technical noise and noise from the stochastic movement of the ribosome, or whether the translation elongation rates themselves must differ among ribosomes to explain the data. In this section we outline the main results, and in next section we provide the technical details.

To characterize the technical noise, we use traces that were not increasing in GFP intensity ("plateau traces"). These traces do not contain noise caused by stochastic movement of the ribosome. We find that the technical noise is well-described by Gaussian white noise, with a variance that scales linearly with the mean spot intensity. Further, we model the ribosome movement along the socRNA as a homogenous one-dimensional Poisson process with a mean rate k. From our description of the system, we can estimate both analytically and through simulation the expected heterogeneity in estimated translation elongation rates $\widehat{k}$, and compare it to the experimental data (Figures 2D and S2A).

Figure S2A shows a scatterplot of the estimated starting length of the polypeptide chain $\widehat{x}_0$ and the estimated translation elongation rate $\widehat{k}$. These estimators are obtained by performing a least-squares linear regression on the single-ribosome translation traces ("moving traces"). Appropriately adjusting for units, $\widehat{x}_0$ and $\widehat{k}$ correspond to the y-intercept and slope of the linear fit, respectively. On the same plot, we superimpose the distribution $p(\widehat{k}|x_0)$, which we obtained analytically. This shows the distribution of $\widehat{k}$ that we expect from our model given a particular starting length x_0.

In Figure 2D, we show the histogram of translation elongation rates $\widehat{k}$ estimated from the moving traces in red. To compare it to our analytical prediction, we integrate out dependence on $\widehat{x}_0$ by computing the distribution $\langle p(\widehat{k}|x_0)\rangle_{x_0}$. This distribution is shown as the blue line in Figure 2D. As an internal consistency check (and to verify our analytical results) we simulated the ribosome movement and added technical noise. The blue histogram in Figure 2D shows the spread in translation elongation rates $\widehat{k}$ from the simulation, and indeed the analytical distribution matches our simulation results. We observe that the spread in estimated translation elongation rates $\widehat{k}$ is significantly wider in the data than would be expected from technical noise and noise from stochastic movement alone. This indicates that there are intrinsic differences between the mean translation elongation rates k of different ribosomes.

On a final note, we should consider the possibility that modelling the ribosome movement as a Poisson process is invalid. In particular, the ribosome is known to cycle through a series of internal protein configurations between successive steps along the RNA, which can cause the number of steps in a given time interval to no longer be Poisson-distributed. A more detailed description of ribosome kinetics from existing models could be incorporated. However, we are in a regime where the central limit theorem suppresses noise caused by the stochastic movement of the ribosome, and the noise is dominated by technical noise. Hence, we do not expect that choosing different movement statistics for the ribosome will significantly impact the conclusions drawn here.

Theoretical methods overview

Here we provide the technical details for the result shown in the above section. Our goal is to find out whether the distribution of estimated translation elongation rates $\widehat{k}$ can be explained by a combination of technical noise and noise from the stochastic movement of the ribosome, or whether the rates themselves are heterogenous. We begin by characterising the noise in the experiment in characterizing the noise in the system, which we use to build a stochastic description of the system. Finally, in distribution of ribosome translation rates, we use least-squares regression to obtain the ribosome translation elongation rates from the moving traces and compare the results we get to those expected analytically from our stochastic picture.

Characterizing the noise in the system

We consider two sources of noise. Firstly, we consider noise due to the stochastic movement of the ribosome. We choose to model the movement as a one-dimensional Poisson process, but we motivate that our results are not model-specific. Secondly, we fully characterize the technical noise using the plateau traces that contain no noise from the movement of the ribosome. Finally, we use our results to formulate a stochastic description of the system.

Ribosome movement: To determine how the stochastic movement of the ribosome contributes to the noise, we require a model for its movement statistics. A kinetic description of ribosome translation can be complicated, involving transitions through multiple configurations of the ribosome between each step and recruitment of the appropriate proteins.[50,51] However, in the experiment, spot intensity is sampled every 1.5 minutes. During this time ~200 codons have been traversed by the ribosome on average. Hence, by the central limit theorem, the statistics of the ribosome movement becomes Gaussian, and we will see that finer details of the kinetic description are averaged out in this regime.

We begin by assuming that the ribosome movement $x(t)$ can be modelled as a homogenous Poisson process with a mean rate k and initial condition $x(0) = x_0$ (Figure S2B). We can write:

$$x(t) = x_0 + kt + \eta(t), \qquad \text{(Equation 1)}$$

Cell

where $\eta(t)$ is the noise, which is Gaussian due to the central limit theorem. We have by construction:

$$\langle x(t) \rangle = x_0 + kt, \tag{Equation 2}$$

$$\langle \eta(t) \rangle = 0,$$

where the angled brackets $\langle \cdot \rangle$ denote the ensemble average. Due to the Poisson statistics, the variance of this process will scale as its mean, meaning that

$$\langle \eta(t)^2 \rangle = kt. \tag{Equation 3}$$

We should consider the possibility that the movement of the ribosome may occur at a mean rate k but is not a Poisson process. One can, in principle, introduce a more detailed kinetic description for ribosome translation and investigate how this impacts the noise. For example, the ribosome is known to transition through multiple internal protein configurations between each step.[7,51] Under the constraint that the ribosome moves with an overall rate k, one can show that introducing additional (Poisson-distributed) intermediate transitions between each ribosome step will decrease the variance compared to Equation 3. One could also consider transitions to a "pausing" state due to, for example, kinetic proofreading. Such processes could increase the variance in Equation 3 while keeping the mean rate k fixed. To proceed, we use a more general argument to argue that due to the central limit theorem, we can continue our analysis without subscribing to a specific kinetic description.

Let the time taken for a ribosome to take one step be denoted by a random variable $T^{(1)}$. Then, we can define the mean time for one step to occur with $E[T^{(1)}] = 1/k$, and its variance with $Var[T^{(1)}] = (\sigma_t^{(1)})^2$. Next, we assume the ribosome steps are independent. Using the central limit theorem, one finds that the noise $\eta(t)$ in the movement of the ribosome is Gaussian, with a variance that is given by:

$$\langle \eta(t)^2 \rangle = kt \left(k \sigma_t^{(1)} \right)^2. \tag{Equation 4}$$

One quick way to see this is by propagating the fluctuations in the time between steps $\sigma_t^{(1)}$ to fluctuations in the ribosome position $\sigma_x^{(1)}$, using $\sigma_x^{(1)} = (dx/dt) \sigma_t^{(1)}$. After kt steps, we get $\langle \eta(t)^2 \rangle = kt(\sigma_x^{(1)})^2$ for the variance and Equation 4 follows. One can check that setting $\sigma_t^{(1)} = 1/k$ recovers the Poisson case above.

We notice that due to the central limit theorem, the only features from the distribution for $T^{(1)}$ that emerge are the mean rate k and variance $\sigma_t^{(1)}$. Hence, as we see from Equation 4, choosing a particular kinetic description only enters our analysis by scaling the noise $\eta(t)$. In section stochastic description of the system, we will see that the technical noise $\xi(t)$ dominates $\eta(t)$. Given that $\eta(t)$ is sub-dominant, we do not expect that choosing different movement statistics will impact the conclusion that the ribosome movement occurs at heterogeneous rates.

Technical noise: To characterize the technical noise, we use the "plateau traces". Here, we have no noise from stochastic movement of the ribosome, and hence the intensity $I(t)$ should fluctuate around a constant value, which we can denote by ax_0:

$$I(t) = ax_0 + \xi(t), \tag{Equation 5}$$

where $a = 1/64.2$ a.u. per amino acid, $\xi(t)$ is the technical noise, and x_0 denotes the (here unchanging) length of the polypeptide chain. We have:

$$\langle I(t) \rangle = ax_0, \tag{Equation 6}$$

$$\langle \xi(t) \rangle = 0,$$

and hence

$$I(t) - \langle I(t) \rangle = \xi(t). \tag{Equation 7}$$

We can therefore gain direct insight into the technical noise by considering deviations from the mean intensity, as in Equation 7.

The data is discretely sampled from the continuous system in Equation 5. Each plateau trace I_j is sampled at N discrete times t_i, with $i = 1,\ldots,N$. We denote the estimated mean intensity from the jth plateau trace as $\widehat{I}_{j,0} = \sum_i I_j(t_i)/N$. From the data, we notice that the noise is Gaussian. Figure S2C shows a histogram in blue of the residuals, $r_j(t_i) = I_j(t_i) - \widehat{I}_{j,0}$, from all plateau traces, normalized to unit variance. A normal distribution with unit variance, shown in red, provides a very good fit. To see if the technical noise has correlations, we compute the autocorrelation for the residuals from each plateau trace. Figure S2D shows a superposition of all the autocorrelation functions, which displays a sharp, central peak. Hence the noise is approximately white. Finally, we have to consider how

the variance scales with the spot intensity $\widehat{I_0}$. We can see in Figure S2E that the variance scales linearly with the spot intensity. Combining these observations, the correlation function of the technical noise is given by:

$$\langle \xi(t)\xi(t') \rangle = \sigma_\xi^2 a(x_0 + kt)\delta(t - t'). \tag{Equation 8}$$

where $\sigma_\xi^2 \approx 0.57$ a.u., corresponding to the slope of the line in Figure S2E. We have also implicitly used the fact that fluctuations in $x(t)$ are small compared to $\langle x(t) \rangle$.

Stochastic description of the system: In order to model the SunTag intensity observed in the experiment, we need to combine our model of the ribosome movement with the technical noise. As above, we denote the observed spot intensity by $I(t)$, measured in units of GFP fluorescence intensity (a.u.). The number of codons traversed by the ribosome is given by $x(t)$, and the additive technical noise is denoted by $\xi(t)$. The observed intensity can then be written as:

$$I(t) = ax(t) + \xi(t), \tag{Equation 9}$$

where $a = 1/64.2$ a.u. per amino acid. If the starting position of the ribosome (or, equivalently, the starting length of the polypeptide chain) is $x(0) = x_0$, we can write

$$x(t) = x_0 + kt + \eta(t), \tag{Equation 10}$$

where $\eta(t)$ captures Gaussian noise from the stochastic movement of the ribosome, as described in section ribosome movement.

Substituting $x(t)$ from Equation 10 into Equation 9, we can describe the system in continuous time with:

$$I(t) = a(x_0 + kt) + a\eta(t) + \xi(t), \tag{Equation 11}$$

where the covariances of $\eta(t)$ and $\xi(t)$ are given by

$$\langle \eta(t)\eta(t') \rangle = kt \tag{Equation 12}$$

for $t \leq t'$, and

$$\langle \xi(t)\xi(t') \rangle = \sigma_\xi^2 a(x_0 + kt)\delta(t - t') \tag{Equation 13}$$

as we saw in sections ribosome movement and technical noise. Further, we assume that the noise terms are independent, i.e. $\langle \xi(t)\eta(t') \rangle = 0$.

Next, we compare the size of fluctuations in $I(t)$ due to the ribosome movement to those due to the technical noise. From Equation 11, one can show that the typical size of the fluctuations in the spot intensity $I(t)$ is given by:

$$\delta I(t) \sim \sqrt{a^2 kt + \sigma_\xi^2 a(x_0 + kt)} \tag{Equation 14}$$

The first term under the square root in Equation 14 is suppressed by an extra factor of a. Hence, in our model, the fluctuations are dominated by technical noise. This is also true for the data, which one can verified by looking at the residuals in the single-ribosome translation traces.

Distribution of ribosome translation rates

In this section, we consider the single-ribosome translation traces. Firstly, in section obtaining translation rates from data, we explain how we estimate the translation rates from the data. Next, in section obtaining translation rates from the stochastic model, we show how to obtain the distribution of ribosome translation rates that one would expect analytically, given our stochastic description of the system. The goal is to compare the heterogeneity in the translation rates from the data to the analytical prediction.

Obtaining translation rates from data: Given a particular intensity trace, we would like to estimate x_0 and k. We denote their respective estimators as $\widehat{x_0}$ and $\widehat{k}$. To do so, we perform a least-squares regression to fit a straight line through each trace. Appropriately adjusting for units, the slopes of these lines correspond to an estimate of the translation rate $\widehat{k}$, and the y-intercept corresponds to an estimate of the starting length $\widehat{x_0}$. A scatterplot of $(\widehat{x_0}, \widehat{k})$ is shown in Figure S2A. Finally, the histogram showing just the distribution of estimated translation elongation rates $\widehat{k}$ is shown as the red histogram in Figure 2D. The details of the least-squares estimator used to perform the regression are shown in the next section.

Obtaining translation rates from the stochastic model: Each trace is sampled at N discrete times t_i, where $i = 1,\ldots,N$. The discrete counterpart of Equation 11 can then be written:

$$I(t_i) = a(x_0 + kt_i) + a\eta(t_i) + \xi(t_i). \tag{Equation 15}$$

Here, $I(t_i)$ contains the measured spot intensity at time t_i. The terms $\eta(t_i)$ and $\xi(t_i)$ contain noise from the stochastic movement of the ribosome and technical noise, respectively.

To estimate $\widehat{x_0}$ and $\widehat{k}$, we use a least-squares regression. To help us, we define the N-by-2 matrix:

$$X = (\mathbf{1} \quad t), \tag{Equation 16}$$

where $\mathbf{1}$ is an N-dimensional vector of ones and $\boldsymbol{t}$ is a vector with elements t_i. Further, we define the parameter vector:

$$\beta = (x_0, kt)^{\mathsf{T}}, \tag{Equation 17}$$

such that Equation 15 can be written in vector notation as:

$$\boldsymbol{I} = a\boldsymbol{X}\beta + a\boldsymbol{\eta} + \xi. \tag{Equation 18}$$

Next, we note that the covariance matrices are given by:

$$(\boldsymbol{S}_\eta)_{ij} = \langle \eta(t_i)\eta(t_j) \rangle = \begin{cases} kt_i, t_i \leq t_j, \\ kt_j, t_i > t_j, \end{cases} \tag{Equation 19}$$

$$(\boldsymbol{S}_\xi)_{ij} = \langle \xi(t_i)\xi(t_j) \rangle = \sigma_\xi^2 a(x_0 + kt_i)\delta_{ij}.$$

This follows directly from the continuous equivalent in Equations 12 and 13. Given that ξ and $\boldsymbol{\eta}$ are independent and Gaussian, we have

$$\boldsymbol{I} \sim \mathcal{N}\left(a(x_0\mathbf{1} + kt), a^2\boldsymbol{S}_\eta + \boldsymbol{S}_\xi\right). \tag{Equation 20}$$

For a given trace $\boldsymbol{I}$, can estimate $\widehat{x}_0$ and $\widehat{k}$ in the least-squares sense by optimising the quantity $\mathcal{L}(\beta) = \|\boldsymbol{I} - a\boldsymbol{X}\beta\|^2$. Setting $\partial\mathcal{L}/\partial\beta = 0$, we obtain the estimator:

$$\widehat{\beta} = \frac{1}{a}(\boldsymbol{X}^{\mathsf{T}}\boldsymbol{X})^{-1}\boldsymbol{X}^{\mathsf{T}}\boldsymbol{I}. \tag{Equation 21}$$

We applied the least-squares estimator in Equation 21 to each of the single-ribosome translation traces to obtain the scatterplot in Figure S2A, as outlined in the previous section.

Next, we want to compare what the distribution of estimators $(\widehat{x}_0, \widehat{k})$ would look like for our stochastic model. To do so, we have to examine the distribution of the estimator $\widehat{\beta}$ itself. This follows straightforwardly from using Equations 20 and 21:

$$\widehat{\beta} \sim \mathcal{N}\left(\beta, \frac{1}{a^2}(\boldsymbol{X}^{\mathsf{T}}\boldsymbol{X})^{-1}\boldsymbol{X}^{\mathsf{T}}(\boldsymbol{S}_\xi + a^2\boldsymbol{S}_\eta)\boldsymbol{X}(\boldsymbol{X}^{\mathsf{T}}\boldsymbol{X})^{-1}\right). \tag{Equation 22}$$

We superimpose the result from Equation 22 in Figure S2A (red). Specifically, on Figure S2A we superimpose the distribution $p(\widehat{k}|x_0)$. This shows, for a given x_0, the expected distribution of translation rates $\widehat{k}$. On top of Figure 2D, we plot the distribution of estimated rates $\langle p(\widehat{k}|x_0)\rangle_{x_0}$. We can clearly see in Figure 2D that technical noise paired with noise from a homogeneous Poisson process is not sufficient to explain the spread in translation rates observed. This indicates that ribosomes are likely to move at different rates.

To test our analytical results, and as an internal consistency check, we simulated the ribosome movement according to our model in Equation 11. The simulated traces were generated to have the same length and starting intensities as the real traces, for fair comparison. The blue histogram in Figure 2D shows the distribution of translation elongation rates obtained from the simulated traces. We can see that the analytical result (blue curve) describes the histogram well, and our analysis is therefore internally consistent.

Supplemental figures
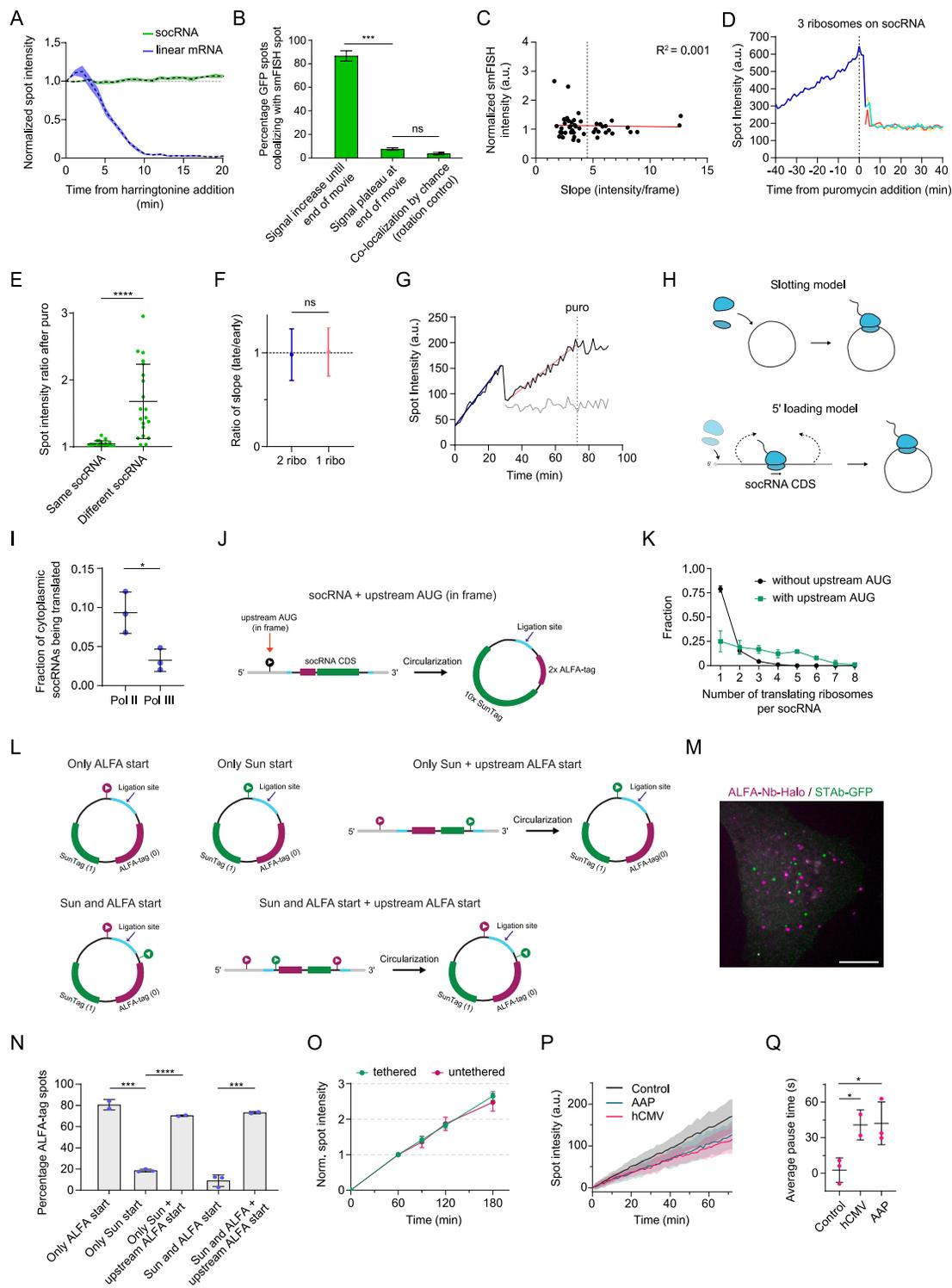
(legend on next page)

Figure S1. Controls for the socRNA translation imaging approach, related to Figure 1

(A) U2OS cells stably expressing STAb-GFP were transfected with either a socRNA (green line) or a linear mRNA encoding 24 copies of the SunTag (blue line) and imaged by time-lapse microscopy. Cells were treated with harringtonine and the intensity of translation site foci was measured over time. Dashed lines represent mean values and shaded regions represent SEM (n = 10 cells).

(B) Cells expressing STAb-GFP and the socRNA were followed by time-lapse analysis and GFP intensity of foci was measured over time. After live imaging, cells were fixed and socRNAs were stained by smFISH. Co-localization of GFP translation foci and smFISH foci was assessed for GFP foci that were increasing in intensity at the end of the time-lapse movie (left bar), or for foci that were not increasing in intensity (middle bar). As a control for random co-localization, the image of one channel was rotated and co-localization was assessed (right bar).

(C) Cells were treated as in (B) and the smFISH foci intensity was plotted against the GFP intensity increase slope. Note that the smFISH intensity was similar between socRNAs with low and high slopes, indicating that the increased slope is not caused by coincidental co-localization of two or more socRNAs translated by single ribosomes. Dashed gray line separates socRNAs translated by single ribosomes (left of line) from socRNAs translated by multiple ribosomes (right of line) as determined in Figure 1K. (n = 2 experiments, 24–26 socRNAs per experiment).

(D) Cells expressing STAb-GFP and a socRNA were followed by time-lapse analysis and GFP intensity of foci was measured over time. Cells were treated with puromycin at t = 0 to release all the nascent chains from the socRNA. Representative intensity time trace of a socRNA translated by three ribosomes. After puromycin addition, three new foci are formed (colored lines) that have identical intensities, indicating that all ribosomes translating the same socRNA initiated translation simultaneously.

(E) Relative intensity differences of spots originating from the same socRNA after puromycin treatment. As a control, we compared intensities of spots originating from different socRNAs. Only translated socRNAs that split into 2–3 foci upon puromycin treatment were included in the analysis (n = 3 experiments, 3–10 socRNAs per experiment).

(F) Ratio between the slope of the first half (early speed) and second half (late speed) of intensity time traces of socRNAs translated by either two (black, 43 socRNAs) or one ribosome (red, 116 socRNAs). Only socRNAs were included for which no ribosomes aborted translation during the experiment. A ratio of 1 indicates that no new ribosomes are loaded on socRNAs during the imaging experiment.

(G) Representative intensity time trace of a socRNA translated by two ribosomes, one of which aborts translation and dissociates from the socRNA (gray line) before puromycin addition (dashed line). Straight lines represent linear fits of the increasing phase during which the ribosome is translated by two (blue line) or one (red line) ribosomes. Note that the slope of the red line is approximately half the slope of the blue line, consistent with a reduction of the number of ribosomes from two to one.

(H) Schematic depicting two possible models by which ribosomes could be loaded onto socRNAs. In the first model, the "slotting model," ribosomes are directly slotted onto socRNA. In the second model, the "5′ loading model," ribosomes are first recruited to the 5′ end of the linear precursor RNA in a cap-dependent mechanism. While the ribosome is translating the coding sequence of the linear precursor RNA, the internal section of the linear RNA becomes circularized, trapping the ribosome in the socRNA.

(I) smFISH was performed to compare the fraction of cytoplasmic socRNAs that are translated when socRNAs are expressed from either a polII or polIII promoter (see STAR Methods). Error bars represent standard deviation from 3 experiments (15–16 cells per experiment).

(J) Schematic of a socRNA encoding 10xSunTag and 2xALFA-tag with an additional AUG in the SunTag translation reading frame positioned in the 5′ UTR of the linear reporter, which is not included in the socRNA after circularization. Cyan regions represent the ribozyme sequences.

(K) The socRNA shown in (J) as well as a second socRNA reporter that is identical except for lacking the indicated upstream AUG were transfected into cells expressing STAb-GFP and ALFANb-CAAX. Shown are the distributions of the number of translating ribosomes for each socRNA. Error bars represent SD from 3 experiments (62–89 socRNAs per experiment).

(L) Schematic of reporters used in (M) and (N). SunTag and ALFA-tag are encoded in distinct reading frames within the socRNA CDS. Colored arrowheads indicate the frame (magenta = ALFA-tag frame, green = SunTag frame) in which the AUG start site is encoded. Cyan regions represent the ribozyme sequences. The RNA region in between the two ribozymes in the linear mRNA will end up in socRNA after RNA circularization. In the two reporters on the right, a schematic of both the linear and circular form of the RNA is shown to indicate the position of an additional AUG that was positioned in the 5′ UTR of the linear RNA. This upstream AUG is not present in the socRNA after circularization, so it can only affect the translation reading frame if initiation occurs on the linear mRNA.

(M) Representative image of cell line expressing STAb-GFP and ALFANb-Halo transfected with socRNA shown in (L). Scale bar, 10 μm.

(N) The socRNAs shown in (L) were transfected into cells expressing STAb-GFP and ALFANb-Halo. The number of SunTag and ALFA-tag foci per cell was scored, and the percentage of ALFA-tag foci out of the total number of foci (ALFA-tag + SunTag) is plotted (n = 2–3 experiments per condition, 8–11 cells per experiment).

(O) A control socRNA was transfected into U2OS cells stably expressing either STAb-mSTayGold, TetR and ALFANb-CAAX (tethered) or STAb-mSTayGold and TetR but lacking the ALFANb-CAAX (untethered). socRNA expression was induced using doxycycline for 5 min. 60, 90, 120, or 180 min after induction, puromycin was added, and 20 min later cells were fixed. After fixation, cells were imaged to determine spot intensities. Error bars represent standard deviation from 3 experiments (381–675 socRNA translation products per condition).

(P and Q) U2OS cells stably expressing STAb-GFP, ALFANb-CAAX, and TetR were transfected with indicated socRNAs and imaged by time-lapse microscopy. The pause sequences derived from the human cytomegalovirus (hCMV) gp48 and fungal arginine attenuator peptide (AAP) were introduced into the control socRNA to measure pause duration on these sequences.

(P) SocRNA GFP foci intensity was measured over time. The intensities at the start of the measurement were set to 0. Lines indicate mean values, and shaded regions indicate standard deviation from 13–51 socRNAs per condition.

(Q) Pause durations at indicated pause sequences were calculated (see STAR Methods). Each dot represents data from an independent experiment (n = 2–3 experiments, 28–96 socRNAs per experiment). Horizontal lines and error bars represent mean ± SD.

*, ***, and **** denotes $p < 0.05$, 0.001, and 0.0001, respectively, determined by t test.

Figure S2. Heterogeneity in single-ribosome elongation speed, related to Figure 2

(A) A scatterplot of estimators $(\widehat{x}_0, \widehat{k})$, estimated from the single ribosome translation traces. The analytical prediction $p(\widehat{k}|x_0)$ from the model is shown in blue. The darkest shade of blue corresponds to σ, the next lighter shade to 2σ, and so forth.

(B) A Poisson counting process $x(t)$ with mean rate k amino acids per second and initial condition $x(0) = x_0$. The number of steps taken by the ribosome in a given time interval is assumed to be Poisson-distributed.

(C–E) The technical noise can be described by Gaussian white noise.

(C) A histogram of residuals $r_j(t_i) = I_j(t_i) - \widehat{I}_{j,0}$, normalized to unit variance, from all plateau traces shows that the technical noise is Gaussian.

(D) The autocorrelation functions $c_j(\tau) = \sum_i r_j(t_i + \tau)r_j(t_i)$ are sharply peaked at $\tau = 0$, implying that there are no temporal correlations; this means the noise is white.

(E) The variance of the technical noise scales linearly with the mean spot intensity.

(F) Single-ribosome translation speeds were plotted against the expression levels of the STAb-GFP in single cells. No correlation between STAb-GFP expression levels and calculated translation elongation rates was observed (241 socRNAs from 3 experiments).

(G) 10xSunTag socRNAs were sequenced using Sanger sequencing (see STAR Methods). Three separate sequencing reactions were performed to sequence the 10xSunTag array, the circRNA ligation junction (presented here) and the 2xALFA-tag sequence. Cyan arrow denotes the socRNA ligation site after circularization. Note that only a single nucleotide was present in the sequencing reaction, indicating that the socRNAs expressed in cells mostly have the same (correct) sequence.

(H) The mobility (mean squared displacement, MSD) of translated socRNAs was assessed. Each dot represents one socRNA translated by a single ribosome. No correlation between socRNA mobility and translation elongation rates was observed (80 socRNAs from 3 experiments).

(I) Average GFP intensity over time for all socRNAs combined (black line) and linear fit (red line). Shaded areas around black line represents the standard deviation. The intensities at the start of measurement were set to 0 (175 socRNAs from 6 experiments).

(J) Deviation of the experimental data in (I) from the linear fit over time. Note that the data do not deviate more from the linear fit at later time points, demonstrating that ribosomes do not slow down during socRNA translation over time.

(K–M) Slope of the first half (early speed) and second half (late speed) of intensity time traces was determined using a linear fit.

(K) Representative intensity time trace and fitting strategy.

(L) Relationship between the elongation rate of the first half and second half of intensity time traces is shown. Spread over the axis of the dashed line ($y = x$) indicates heterogeneity in elongation rates between different translating ribosomes. In contrast, spread over the orthogonal axis ($y = -x$) suggest that ribosomes speed up or slow down during translation of a single socRNA (within trace elongation speed heterogeneity) (106 socRNAs from 3 experiments).

(M) Relationship between the slope of the first half and second half of control intensity time traces is shown (227 socRNAs from 3 experiments).

(N) Average translation elongation speed on individual socRNAs in different cells. Magenta dots represent individual socRNAs translated by one ribosome. All magenta dots in each vertical row are from the same cell. Horizontal black lines represent mean and errors bars represent standard deviations. ANOVA statistical test indicates that average elongation speeds in different cells are not statistically different (54 cells from 3 experiments).

(O) Elongation speed of two randomly selected ribosomes translating different socRNAs within the same cell are plotted (the speed of one ribosome is plotted on the x axis, the other on the y axis). Note that there is little correlation between elongation speeds of ribosomes within the same cell. Spread of points perpendicular to the diagonal dashed line corresponds to the difference in elongation speeds within the same cell.

(P) To correct for photobleaching, GFP intensity time traces of non-translating GFP foci was measured. Red line represents single exponential decay fitting result that was used to correct for photobleaching for all GFP intensity time traces (18 traces).

(Q) Example of photobleaching correction for intensity time trace of translated socRNAs. We corrected photobleaching using the value acquired in (P). Note that after bleach correction GFP intensity showed a plateau upon puromycin treatment, as expected.

(R) Slopes of GFP spot intensity time traces obtained either from increasing traces (single ribosomes translation socRNAs) (magenta, 221 socRNAs), plateau traces (likely polypeptides for which translated has been aborted) (green, 99 socRNAs), and after puromycin treatment (gray, 119 socRNAs). The plateau traces showed a similar slope distribution as the traces acquired after puromycin treatment, confirming that they reflect "non-translating" GFP foci.
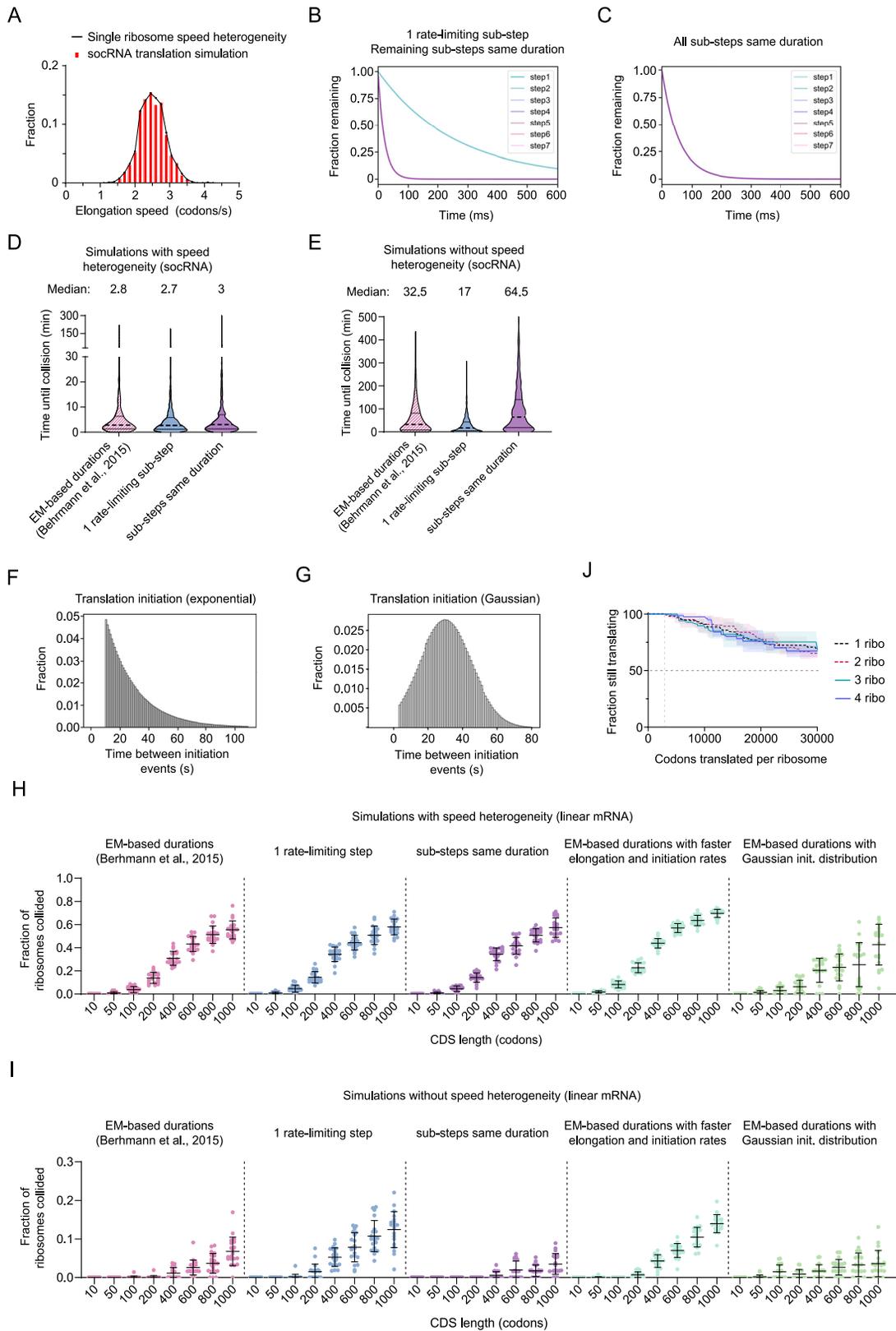
Figure S3. Simulating ribosome collisions on socRNAs and linear mRNAs, related to Figure 2

(A) The distribution of single-ribosome elongation speeds determined experimentally (black line) (replotted from Figure 2C) or from the simulations (red bars; see STAR Methods).

(B and C) Distributions of the duration of each step in the translation elongation cycle used in simulations.

(D and E) The time until the first collision between two ribosomes translating the same socRNA was determined based on simulations. Simulations were repeated 1,000 times for each condition (see Figure 2E; see B and C). Thick dashed line indicates the median, thin lines indicate 25th and 75th percentile. Median values are listed above each graph.

(D) Simulations including ribosome speed heterogeneity were performed for different elongation cycle sub-step regimes to determine the time until 2 ribosomes translating the same socRNA collide. Data showing "EM-based durations" are replotted from Figure 2I.

(E) Simulations without including ribosome speed heterogeneity were performed for different elongation cycle sub-step regimes to determine the time until 2 ribosomes translating the same socRNA collide.

(F) Distribution of time intervals between translation initiation events used in the simulation shown in Figure 2J, and also in 3 out of 5 simulations shown in (H) and (I) (EM-based durations, "1 rate-limiting step," and "sub-steps same duration").

(G) Distribution of time intervals between translation initiation events used in simulations shown in (H) and (I) ("EM-based durations with Gaussian init. distribution").

(H and I) Simulations were performed to determine the frequency of ribosome collisions on mRNA molecules as a function of mRNA coding sequence (CDS) length. Each data point represents a single simulated mRNA molecule, and 20 mRNAs were simulated for each different condition (see Figure 2E and STAR Methods; see B, C, F, and G). Horizontal lines and error bars represent mean ± SD.

(I) Simulations of mRNA translation without intrinsic ribosome speed heterogeneity were performed to determine the fraction of ribosomes undergoing at least one collision during translation of the CDS.

(J) U2OS cells stably expressing STAb-GFP, ALFANb-CAAX, and TetR were transfected with control socRNAs and imaged by time-lapse microscopy. Kaplan-Meyer survival curves show the total number of codons translated per ribosome before aborting translation for socRNAs translated by either 1, 2, 3, or 4 ribosomes. Black and magenta dashed lines are replotted from Figure 2K. Lines indicate mean values, and shaded regions indicate standard deviation (n = 2–3 experiments, 29–85 ribosomes per experiment).
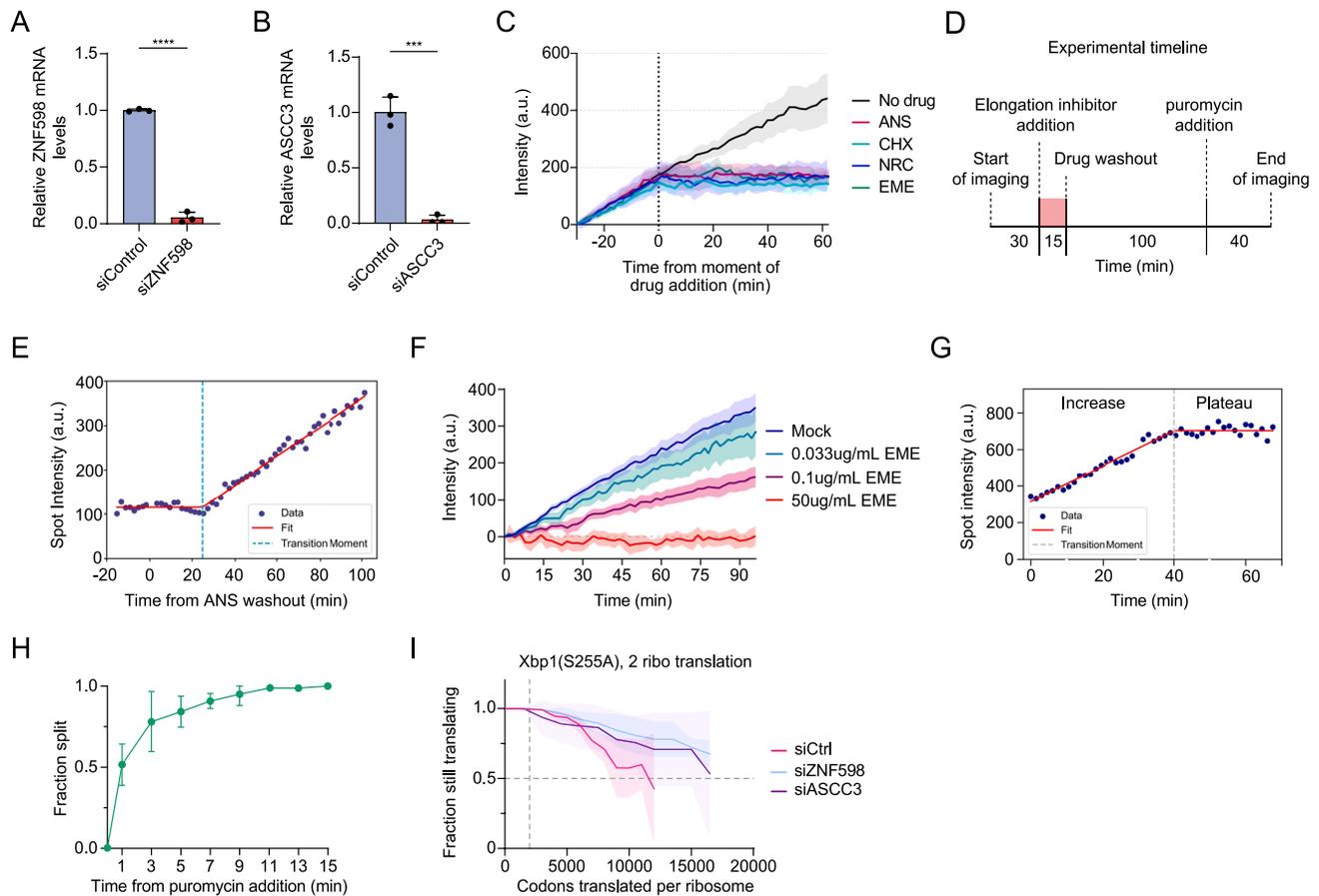
Figure S4. Controls for investigating ribosome collisions and recycling, related to Figure 3

(A and B) Quantitative PCRs were performed to assess the knockdown efficiency of siRNA treatment for ZNF598 (A) and ASCC3 (B). *** and **** indicate $p < 0.001$ and 0.0001, respectively, determined by t test. Dots represent the data from independent experiments. Error bars represent mean ± SD.

(C) U2OS cells were treated with the translation elongation inhibitors explored in Figures 3K–3O. Without drug washout, translation elongation does not resume after drug addition ($n = 2$ experiments, 4–10 socRNAs per experiment).

(D) Overview of the experimental setup used in and Figures 3K–3O.

(E) Representative example of data fitting approach for trace shown in Figure 3L to identify the moment that translation resumes after translation pausing induced by ribosome-targeting drugs.

(F) U2OS cells stably expressing STAb-GFP, ALFANb-CAAX, and TetR were transfected with control socRNAs and imaged by time-lapse microscopy. Emetine was added at different concentrations to determine the dose-dependent effect on average protein synthesis rates by single translating ribosomes. Lines indicate mean values, and shaded regions indicate 95% of CI ($n = 1$–2 experiments, 9–21 socRNAs per experiment).

(G) Representative example of data fitting approach to identify the plateau duration preceding the moment of ribosome recycling for trace shown in Figure 3P.

(H) U2OS cells stably expressing STAb-GFP, ALFANb-CAAX, and TetR were transfected with control socRNAs and imaged by time-lapse microscopy. Puromycin was added to cells to determine the time needed for nascent chains from socRNAs translated by two ribosomes to visibly dissociate from each other. Fitting with a single exponential function reveals a half-life of 1.4 min ($n = 2$ experiments, 33–40 socRNAs per experiment).

(I) U2OS cells stably expressing STAb-GFP, ALFANb-CAAX, and TetR were transfected with indicated socRNAs and siRNAs and imaged by time-lapse microscopy. Kaplan-Meyer survival curves of indicated socRNAs show the total number of codons translated by individual ribosomes before aborting translation. Lines indicate mean values, and shaded regions indicate standard deviation from 4 independent experiments (6–30 socRNAs per experiment).
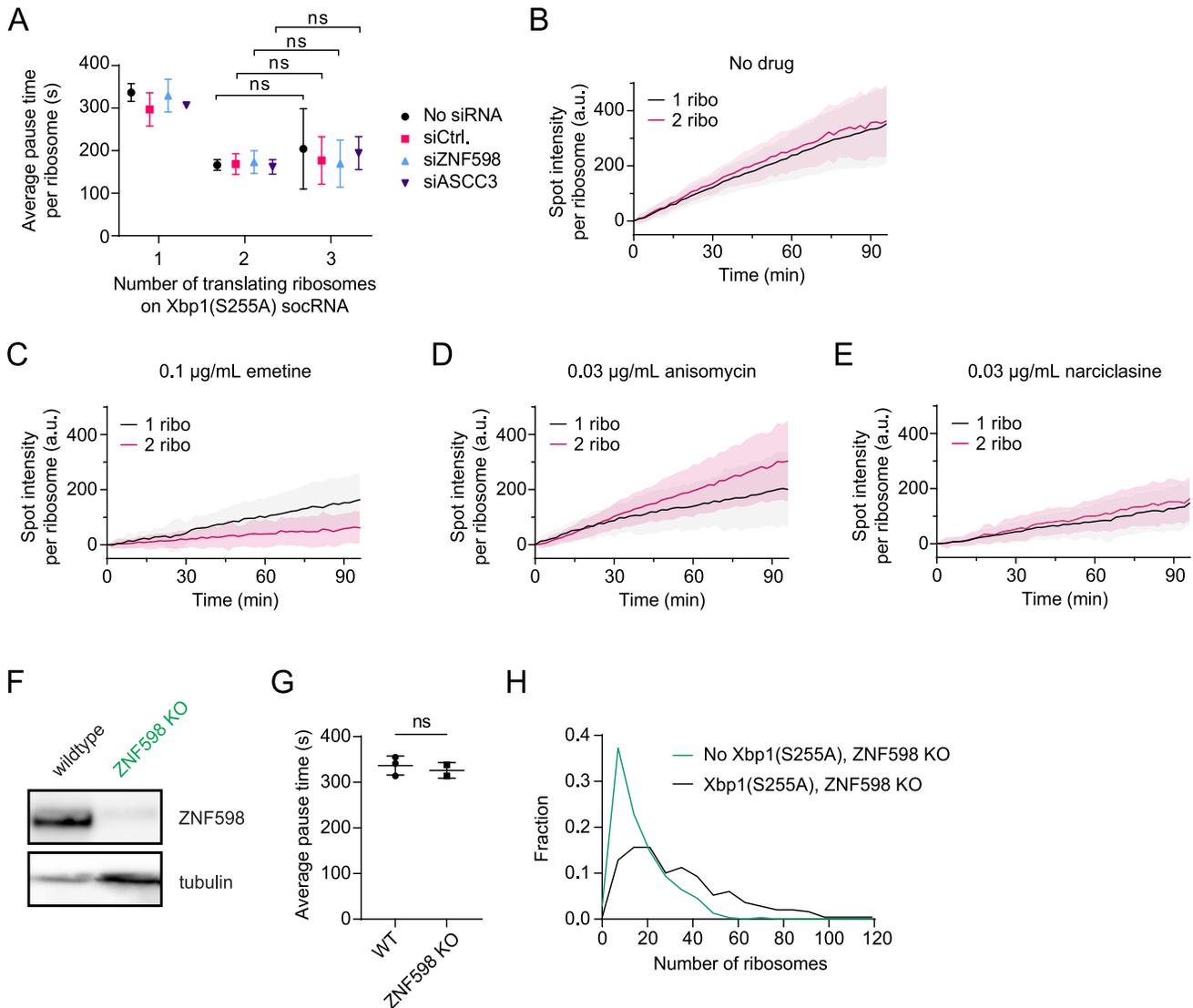
Figure S5. Controls for ribosome cooperativity, related to Figure 4
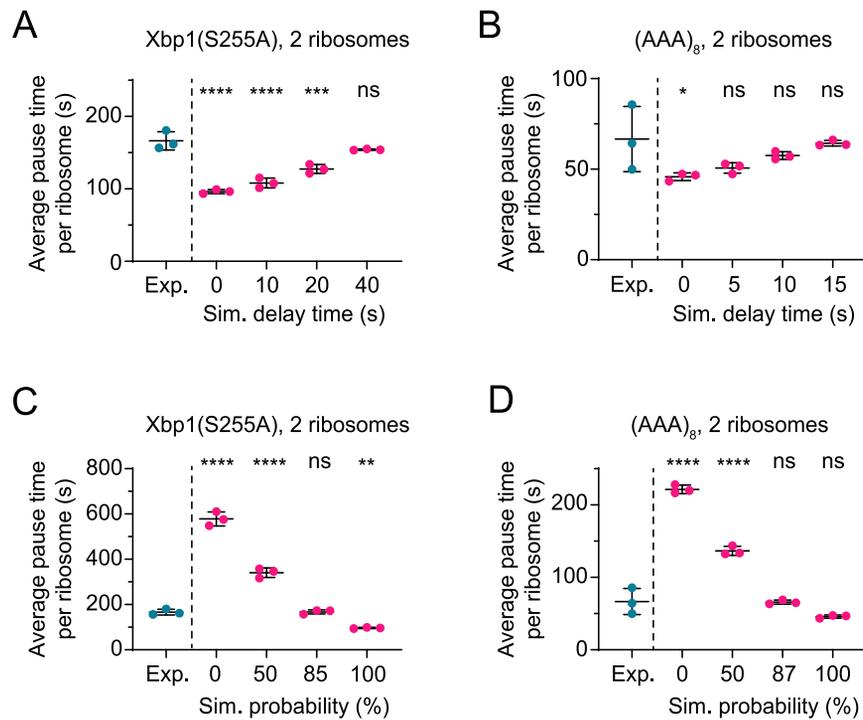
(A) Average pause duration at the Xbp1(S255A) pause sequence was calculated using GFP intensity time traces for socRNAs translated by one, two, or three ribosomes (*n* = 3 experiments, 3–29 socRNAs per condition). No significant difference in pause duration was observed between the socRNAs translated by either two or three ribosomes.

(B–E) U2OS cells stably expressing STAb-GFP, ALFANb-CAAX, and TetR were transfected with socRNAs and imaged by time-lapse microscopy. Cells were treated with indicated low concentrations of elongation inhibitors to determine the effect of drug-induced pausing on ribosomes translating a socRNA either alone or together with a second ribosome. socRNA spot intensities were measured over time and normalized to the number of ribosomes on the socRNA for direct comparison (see STAR Methods). Lines indicate mean values and shaded regions indicate standard deviation from 3–4 experiments (number of socRNAs [1 ribo, 2 ribo] = 86, 56 in A; 74, 44 in B; 78, 56 in C; 85, 53 in D).

(F) Parental or ZNF598 knockout cells were lysed and western blots were performed to assess the levels of ZNF598 protein. Note that a non-specific band is apparent immediately above the ZNF598 band, which is still visible in the ZNF598 KO sample.

(G) Average pause duration at the Xbp1(S255A) pause sequence was calculated using GFP intensity time traces for socRNAs translated by a single ribosome (*n* = 2 experiments, 23–25 socRNAs per experiment). No significant difference in pause duration was observed between WT and ZNF598 knockout cells. Data of WT cells is replotted from Figure 3E for comparison.

(H) Distribution of the number of ribosomes translating the linear mRNA reporter shown in Figure 4K, either with or without the Xbp1(S255A) pause sequence (2 experiments, number of mRNAs = 249 for Xbp1[S255A], 311 for no Xbp1[S255A]).

Figure S6. Simulation of ribosome cooperativity, related to Figure 5

(A–D) Simulation of the average pause duration on Xbp1(S255A) (A and C) or $(AAA)_8$ (B and D) pause sequences for socRNAs translated by two ribosomes. Collision-induced resumption of translation of the paused ribosome was simulated for two different ribosome cooperativity models. Cyan (experimental data) dots are replotted from Figures 5A and 5B for comparison. Horizontal lines and error bars represent mean ± SD.

(A and B) Different delay times between the moment of collision and resumption of translation of the paused ribosome were simulated.

(C and D) For each collision between a translocating ribosome and a ribosome paused on indicated pause sequences a probability was simulated that the collision resulted in resumption of translation. A probability of 0% means that no ribosome cooperativity was included.

*, **, ***, and **** indicate $p < 0.05$, 0.01, 0.001, and 0.0001, respectively, determined by t test. The dots represent the data from independent experiments or simulations.
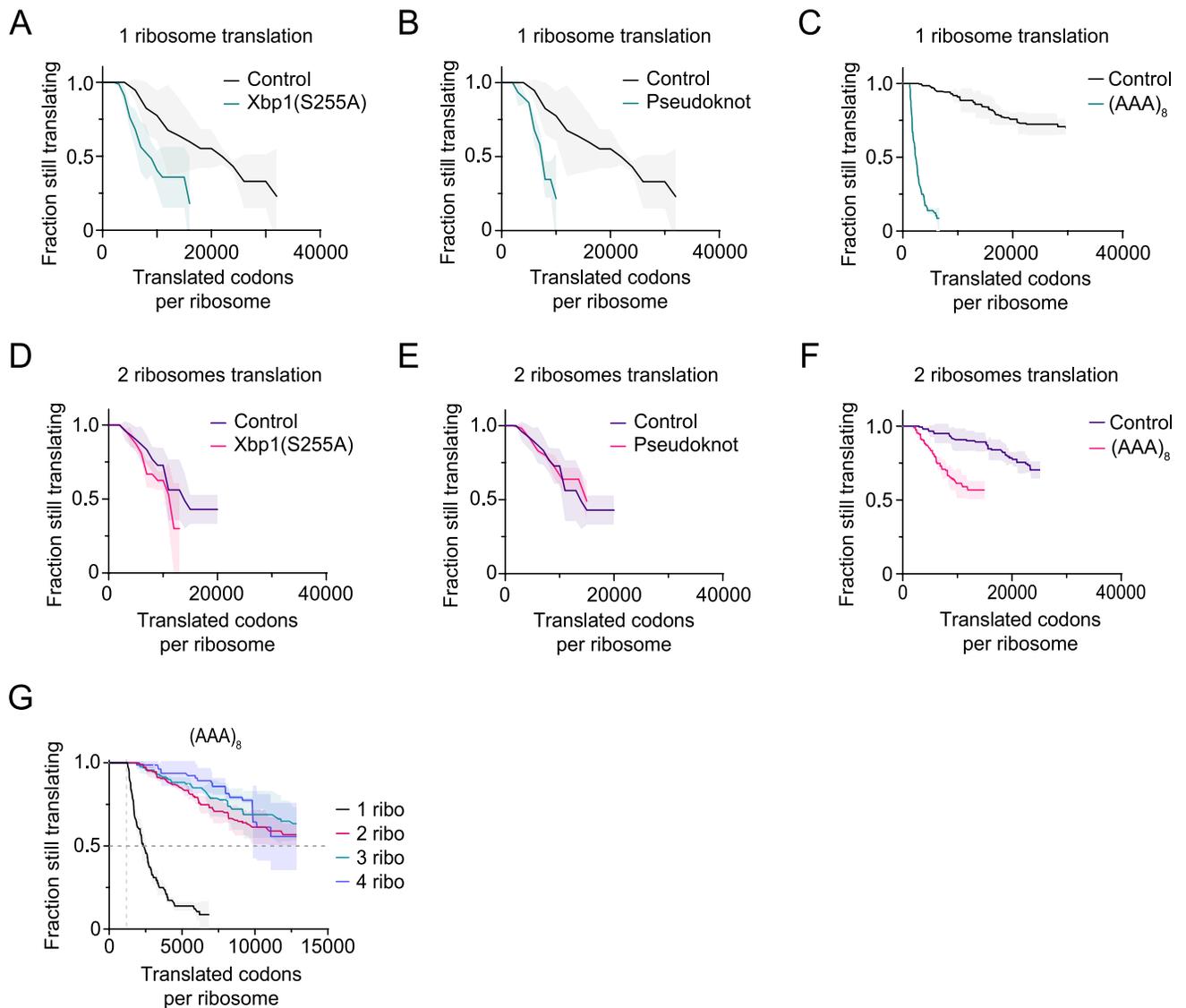
Figure S7. Ribosome cooperativity enhances processivity, related to Figure 6

(A–F) U2OS cells stably expressing STAb-GFP, ALFANb-CAAX, and TetR were transfected with indicated socRNAs and imaged by time-lapse microscopy. Kaplan-Meyer survival curve of indicated socRNAs shows the total number of codons translated by individual ribosomes before aborting translation. Xbp1(S255A) (A and D), Pseudoknot (B and E), and (AAA)$_8$ (C and F) data are replotted from Figures 6A–6C for comparison. Lines indicate mean values, and shaded regions indicate standard deviation of 2–3 experiments (10–39 socRNAs per experiment).

(G) U2OS cells stably expressing STAb-GFP, ALFANb-CAAX, and TetR were transfected with indicated socRNAs and imaged by time-lapse microscopy. Kaplan-Meyer survival curves of indicated socRNAs show the total number of codons translated by ribosomes before aborting translation. Lines indicate mean values, and shaded regions indicate standard deviation determined from 3 experiments (6–36 socRNAs per experiment).